View metadata, citation and similar papers at core.ac.uk

brought to you by CORE

provided by NASA Technical Reports Server

Mid-IR Properties of an Unbiased AGN Sample of the Local Universe. I. Emission-Line Diagnostics

K. A. Weaver, M. Melendez[1,2], R. F. Mushotzky, S. Kraemer[3], K. Engle[4], E. Malumuth[5], J. Tueller, C. Markwardt[6]

NASA Goddard Space Flight Center, Greenbelt, MD, 20771

C.T. Berghea[7] and R. P. Dudik

U.S. Naval Observatory, Washington, DC 20392

L. M. Winter[8]

Center for Astrophysics and Space Astronomy, University of Colorado, Boulder, CO

and

L. Armus

Spitzer Science Center, California Institute of Technology, Pasadena, CA

Received _____; accepted _____

---

[1]NASA Postdoctoral Program Fellow, Goddard Space Flight Center, Greenbelt, MD, 20771

[2]present address: Department of Physics and Astronomy, John Hopkins University, Baltimore, MD, 21218

[3]Institute for Astrophysics and Computational Sciences, Department of Physics, The Catholic University of America,Washington, DC

[4]Adnet

[5]SESDA

[6]University of Maryland, College Park, MD

[7]Computational Physics, Inc., Sprinfield, VA 22151

[8]Hubble Fellow

To be submitted to the Astrophysical Journal

ABSTRACT

We compare mid-IR emission-lines properties, from high-resolution *Spitzer* IRS spectra of a statistically-complete hard X-ray (14 – 195 keV) selected sample of nearby ($z < 0.05$) AGN detected by the Burst Alert Telescope (BAT) aboard *Swift*. The luminosity distribution for the mid-infrared emission-lines, [O IV] 25.89 μm, [Ne II] 12.81 μm, [Ne III] 15.56 μm and [Ne V] 14.32 μm, and hard X-ray continuum show no differences between Seyfert 1 and Seyfert 2 populations, although six newly discovered BAT AGNs are shown to be under-luminous in [O IV], most likely the result of dust extinction in the host galaxy. The overall tightness of the mid-infrared correlations and BAT luminosities suggests that the emission lines primarily arise in gas ionized by the AGN. We also compared the mid-IR emission-lines in the BAT AGNs with those from published studies of star-forming galaxies and LINERs. We found that the BAT AGN fall into a distinctive region when comparing the [Ne III]/[Ne II] and the [O IV]/[Ne III] quantities. From this we found that sources that have been previously classified in the mid-infrared/optical as AGN have smaller emission line ratios than those found for the BAT AGNs, suggesting that, in our X-ray selected sample, the AGN represents the main contribution to the observed line emission. Overall, we present a different set of emission line diagnostics to distinguish between AGN and star forming galaxies that can be used as a tool to find new AGN.

Subject headings: AGN: general – galaxies: Seyfert – X-rays – IR

1. Introduction

Active galactic nuclei span over seven orders of magnitude in bolometric luminosity (L_{bol}) (Koratkar & Blaes 1999) and yet are all believed to be powered by the same physical mechanism: accretion of matter onto supermassive black holes. To learn why there is such a large range in AGN activity and how AGN interact with their host galaxy, it is crucial to directly measure their effect on their host galaxy and to understand the relative role of star formation. This requires eliminating selection bias as much as possible.

We are examining the properties of host galaxies in concert with their AGN by concentrating on a hard-x-ray selected sample of AGN in the local Universe (e.g. $z < 0.05$). Studies of nearby AGN have tended to focus on Seyfert galaxies, which are modest luminosity AGN ($L_{bol} \lesssim 10^{45}$ erg s^{-1}), but bright enough to be examined across the full electromagnetic spectrum. Type I objects are those which possess broad, optical permitted emission lines (Full Width Half Maximum (FWHM) $\gtrsim$ several 1000 km s^{-1} and narrower forbidden lines (FWHM $\lesssim$ 1000 km s^{-1}) and non-stellar optical continua. Type II objects possess permitted and forbidden optical emission lines of similar narrow widths and their optical continua are dominated by the host galaxy. The broad permitted lines come from a region light-days in size (e.g., Peterson et al. 2004) and, hence, cannot be resolved with current optical instrumentation, while the narrow lines come from a more extended region, referred to as the narrow-line region (NLR), hundreds of parsecs in extent. The NLRs of a large number of AGN have been resolved by the *Hubble Space Telescope (HST)* (e.g., Crenshaw & Kraemer 2000; Schmitt et al. 2003).

Although traditionally defined in terms of their optical properties, sample selection of AGN via a single waveband can lead to observational bias (e.g., Mulchaey et al. 1994). For example, most AGN are obscured from our line of sight by dust and gas (Matt 2000) and any selection based on optical (or UV) properties would miss many objects or could highly

skew a sample towards unobscured objects (e.g., Barger et al. 2005). The X-ray properties of Seyfert galaxies generally follow the same dichotomy as their optical properties. The X-ray continuum source in Seyfert 1s can be observed directly, at least at energies > 2 keV (e.g., George et al. 1998), while the central X-ray source is sometimes undetectable in Seyfert 2s, due to material ($> 10^{22.5}$ cm^{-2}) along our line of sight. Therefore, soft X-ray selected samples would be incomplete as well.

There is additionally a wide range of effective IR colors (Kuraszkiewicz et al. 2003; Lutz et al. 2005) which can introduce bias. A comparison of *Spitzer* and X-ray data (Franceschini et al. 2005) shows a factor of 30 range in the IR 24 micron to ~4 keV X-ray flux ratio for X-ray selected AGN, suggesting a range of geometries and optical depths for dust reprocessing, and probably variance in the intrinsic power law AGN continuum. Obscuration and star formation in the host galaxy can also dominate and introduce confusion in the IR emission (e.g., Lutz et al. 2004; Barmby et al. 2006). In fact, virtually all surveys for AGN based purely on IR, optical, UV or soft X-ray data have been biased (Mushotzky 2004). Even Sloan surveys (Heckman et al. 2004) or *Spitzer* IR surveys (Franceschini et al. 2005) have required indirect AGN indicators which are known to be not necessarily robust (Meléndez et al. 2008a).

To understand the intrinsic properties of AGN as a class, it is critical to start with a survey where we can be as certain as possible that we are viewing the AGN-only parts of these galaxies. At X-ray energies of $E > 10 - 20$ keV, the obscuring material is relatively optically thin for column densities less than $\sim 3 \times 10^{24}$ cm^{-2} (Compton-thin objects). Even if an AGN is well buried within its host galaxy there is an unaffected view of the central power source. A hard X-ray survey should thus find all Compton thin AGN in a uniform fashion and is the most unbiased, since at present, there are very few, if any, known X-ray "quiet" AGN. Such a hard X-ray survey is now available from the *Swift* Burst Alert

Telescope (BAT). The BAT detects all bright AGN, whether they are obscured or not, and finds famous classical objects as well as previously unknown or poorly studied AGN. Several of the BAT sources are newly discovered AGN, which have been poorly studied, if at all, at other wavelengths (Winter et al. 2008; Tueller et al. 2008, 2009).

Examining the IR properties of the BAT-detected AGN will provide insight into the IR/X-ray scatter and help determine the true distribution of IR properties. Therefore, we have obtained *Spitzer* Space Telescope spectra of the BAT sample of nearby AGN. Combining the hard X-ray fluxes from the BAT with the *Spitzer* spectra will allow us to deconvolve the contributions of star formation and the AGN to the mid-IR emission lines. Furthermore, since we are studying AGN with well-constrained luminosities, via the hard X-ray, we can determine which mid-IR lines result from truly isotropic quantities, which can, in turn, be used to constrain the power of AGN that are too faint to be detected in the X-ray (e.g., Compton thick sources). Moreover, the mid-IR lines can penetrate the dust that can affect optical emission line diagnostics, such as [O III] λ5007 (e.g., Meléndez et al. 2008a; Winter et al. 2010).

There have been a large number of studies of the mid-infrared emission line properties of galaxies using both *Infrared Space Observatory* (Kessler et al. 1996) and *Spitzer Space Telescope* (Werner et al. 2004). The ratios of high- and low-ionization mid-infrared emission lines have been widely used to separate the relative contribution of the AGN and star formation (Genzel et al. 1998; Sturm et al. 2002; Dale et al. 2006; Armus et al. 2007; Farrah et al. 2007; Meléndez et al. 2008b, e.g.,). More recently, Hao et al. (2009) (H09) used new high-resolution *Spitzer* spectroscopy to probe the utility of mid-infrared emission line diagnostics as a way to separate active galaxies from star forming galaxies. In our first study of mid-infrared properties of the BAT AGNs (Meléndez et al. 2008a), we found the [O IV]25.89μm to be an accurate indicator of the AGN luminosity, with an uncertainty of

$\sim$0.3 dex; this result was confirmed in more recent studies using a larger sample (Rigby et al. 2009; Diamond-Stanic et al. 2009). Using a complete, volume-limited, sample of galaxies Goulding & Alexander (2009) (GA09) demonstrated the utility of mid-infrared emission lines, such as [Ne V]14.32μm, to identify AGN including those that were not identified as AGN in optical studies (see also, Landi et al. 2007; Abel & Satyapal 2008; Dudik et al. 2009; Satyapal et al. 2009). Similar results have been found by Bernard-Salas et al. (2009) (B09) in their study of starburst galaxies. Based on all of these studies, these line diagnostics will be particularly useful to analyze spectra from new IR missions, such as the *James Webb Space Telescope*.

This paper is the first in a series seeking to understand the nature of the observed IR luminosities in AGN and their wide variety of spectral forms. Here we report results from the portion of our sample that have high-resolution *Spitzer* spectra. This work complements the extensive optical imaging and spectroscopy of the AGN population (Koss, in preparation; Winter et al. 2010) and the detailed analysis of the X-ray properties of the BAT AGN sample (e.g., Winter et al. 2008, 2009a,b). In following papers we will report on the results from our analysis of the low-resolution *Spitzer* spectra which will include the study of polycyclic aromatic hydrocarbon (PAH) features, molecular Hydrogen emission, silicate absorption and mid-infrared continuum properties of the BAT AGN sample. In order to calculate the luminosities presented in this work we assume a flat universe with a Hubble constant $H_o = 71 \mathrm{kms}^{-1}\mathrm{Mpc}^{-1}$, $\Omega_\Lambda = 0.73$ and $\Omega_\mathrm{M} = 0.27$, with redshift values taken from NASA's ExtraGalactic Database (NED).

2. Observations and Analysis

2.1. X-ray data and AGN sample selection

Our sample was selected from the first unbiased local AGN sample obtained with the Swift Burst Alert Telescope (BAT) survey. The Swift BAT is sensitive over ~85% of the sky to a flux threshold of 2×10^{-11} ergs cm^{-2}s^{-1} in the 14−195 keV band (Markwardt et al. 2005). The BAT data are about 10 times more sensitive than the previous hard X-ray all sky survey (Levine et al. 1984). The X-ray positions have $\sim 3''$ positional uncertainties and we are highly confident of the positions and the optical identifications. Source identifications are based primarily on the X-ray imaging data and a correlation with optical images and catalogs. In some cases the identifications are based on positional coincidences with previously known AGN.

The median redshift of the BAT objects is $z \sim 0.025$. Our selection criteria are $z < 0.05$, $|b| > 19°$ and a hard X-ray BAT flux of > 2 x 10^{-11} erg cm^{-2} s^{-1}. The flux limit provides sufficient S/N to be sure that the sources are statistically robust. Our total BAT sample contains 130 objects above a significance threshold of 5.0 σ. We obtained from the Infrared Spectrograph (IRS) on board *Spitzer* high and low resolution spectra for sixty of these objects, while seventy previously had *Spitzer* IRS spectra from other observing programs.

In this paper we focus on BAT luminosity as the most reliable indicator of AGN strength. There are published BAT AGN catalogs from two surveys, the 9-month survey (Tueller et al. 2008) and an updated 22-month catalog (Tueller et al. 2009). Here we use the 22-month fluxes from Tueller et al. (2009) as the 22-month survey is the most sensitive. However, in our sample, four of the AGN in the 9-month survey were not detected in the 22-month survey, therefore we will use the fluxes from the 9-month survey as upper-limits

(see footnote in Table 1).

2.2. *Spitzer* Observations and Data Analysis

In this work we discuss only the high-resolution spectroscopy of our total sample, which result on a subsample of 79 BAT AGN that have high-resolution *Spitzer* spectra. The galaxies in our sample were observed with the Infrared Spectrograph (IRS) on board the *Spitzer* in the Short-High (SH, λ = 9.9 - 19.6 μm, 4.7″ × 11.3″,$R \sim 600$) and Long-High (LH, λ = 18.7 - 37.2 μm, 11.1″ × 22.3″, $R \sim 600$) IRS order in staring mode. Science targets in staring mode are placed at two node position along the IRS slit. This sample includes fluxes found in the literature (Weedman et al. 2005; Armus et al. 2006; Tommasin et al. 2008) and from our analysis of unpublished archival spectra observed with IRS, including observations collected with the *Spitzer* Cycle 3 and Cycle 5 GTO program "Spitzer Observations to Complete the First Unbiased AGN Sample of the Local Universe" (P30745 and P50588, PI: K. Weaver). The high-resolution sample includes, 38 Seyfert 1's, 33 Seyfert 2's, 6 previously unknown or poorly-studied AGNs and two LINERs (NGC 4102 and NGC 1052). High resolution spectroscopy allow us to easily separate blended features such as, [O IV] 25.89μm-[Fe II] 25.98μm, [Ne V] 14.32μm-[Cl II] 14.37μm. Moreover, the subsample presented in this work spans the same range on 14-195 keV luminosities as the 22-month BAT AGN sample and is large enough to be statistically representative of the whole sample of 130 AGN, therefore, maintaining the statistical similarities between Seyfert population. Finally, our subsample also have the same range in mid-infrared emission line luminosities than other complete samples as the 12μm (Tommasin et al. 2010) and the revised Shapley-Ames sample (Rigby et al. 2009), suggesting that our subsample is not biased toward high or low luminoues sources.

For the analysis of *Spitzer* data we used the basic calibrated data files preprocessed

using the S17.2 IRS pipeline. This include ramp fitting, dark sky subtraction, drop correction, linearity correction and wavelength and flux calibrations [1]. Many of the sources in our sample have dedicated off-sources observations to do a sky subtraction, which can alleviate the effect of rogue pixels and variable background. Off-sources images were averaged for each node position and order to obtain a final background image. Then, we subtract the sky background from our spectrum. The full slit spectra were extracted from the IRS data using the Spectroscopy Modeling Analysis and Reduction Tool (SMART) v6.4.0 (Higdon et al. 2004). For the extraction we used the "Full Aperture" extraction method for high-resolution observations of point sources. We created median basic calibrated data files from each node and then the spectra from each node position for SH/LH were averaged using 2.5-σ clipping to reject outliers. Finally, we trimmed the edges of the orders to obtain a final clean spectrum. For sources without dedicated off-source observations we did not perform any background subtraction because we only required emission-line fluxes, furthermore, our hard X-ray selected sample is characterized by bright nuclear sources which fill the high-resolution slit resulting in a minimal background correction. We performed the line fit with SMART using a polynomial to fit the continuum and a Gaussian for the line profile. In Table 1 we report the line fluxes, together with their 1-σ statistical error for the whole high-resolution sample. The typical 1-σ statistical errors for the mission lines presented in this work are, on average, $\sim$9%, $\sim$10%, $\sim$5%, $\sim$12% and $\sim$8% for the [Ne II]12.81μm, [Ne V]14.32μm, [Ne III]15.56μm, [Ne V]24.32μm and [O IV]25.89μm emission lines, respectively. From this and for the sake of simplicity we did not plot error bars on individual objects in the different comparisons presented in this work, as the errors are comparable to the symbol size uses in the figures. For non-detections we quote the 3-σ upper limits as defined for emission-lines with a S/N less than 3. Finally, The

[1]See the IRS Pipeline Handbook, http://ssc.spitzer.caltech.edu/irs/dh/irsPDDmar30.pdf

emission-line fluxes are presented here without reddening corrections.

Each of the galaxies in our sample has clearly detected [O IV], [Ne II] and [Ne III] emission. There are a few that do not have detectable [Ne V] 14.32μm and fewer that have [Ne V] 24.31μm. Although a number of other strong emission lines are present in these data, e.g. [S III] 18.7μm, 32.48μm, [S IV] 10.5μm, and [Si II] 34.82μm. The importance of [O IV] and the neon emission lines is that they have been shown to be sufficient to test the source of ionization and distinguish specifically between stellar and AGN activity. The neon line ratios are also tracers that are insensitive to abundance. For example, the [Ne III]/[Ne II] and [O IV]/[Ne II] ratios are good discriminators of star formation and AGN emission (Genzel et al. 1998; Sturm et al. 2002; Satyapal et al. 2004; Meléndez et al. 2008b), while the strengths of [O IV] (Meléndez et al. 2008a; Rigby et al. 2009) and [Ne V] (e.g., Satyapal et al. 2007; Dudik et al. 2007; Abel & Satyapal 2008) scale with the luminosity of the AGN. It should be noted, however, that these latter emission lines can be strong in some classical AGN and not in others (Weedman et al. 2005), possibly due to the shielding of the narrow line region by optically thick, dusty gas close to the AGN (e.g., Armus et al. 2007). According to studies in the literature (GA09) and our own work (Melendez et al., in prep.) the results from either [Ne V] line are similar in terms of their diagnostic potential for AGN and so we here focus here on the stronger [Ne V] 14.32μm line.

3. Mid-IR properties of the BAT sample

3.1. Comparison of the IR Emission-Line and BAT Luminosities

As noted above, via the hard X-ray band we can detect AGN that may have been missed in optical surveys due to the extinction of their optical emission lines. Among the 79 targets present here (BAT AGN), we have found six poorly studied or previously

unknown AGN ("new BAT-detected AGN"): ESO 005-G004, Mrk 18, NGC 973, NGC 4686, UGC 12282, and UGC 12741. Follow-up observations in the optical have attempted to classify some of these galaxies. Of these, ESO 005-G004 has been classified as a Seyfert 2, based on its X-ray properties although no optical AGN signature has been detected (Landi et al. 2007; Ueda et al. 2007). Mrk 18 has an ambiguous classification with HII/LINER properties (Winter et al. 2010) and NGC 973 has been classified as a narrow emission line AGN with Sy2/LINER properties (Masetti et al. 2008). UGC 12282 has been classified as a Sy 1.9 based on its optical spectra (Véron-Cetty & Véron 2006). Finally, to the best of our knowledge there is no assigned classification for NGC 4686 and UGC 12741. The *Spitzer* IRS spectra of these objects are shown in Figure 1.

In Figures 2 – 7 we compare the mid-IR emission lines and the BAT luminosities, correlations between the emission lines, and emission line ratios. The statistical analysis for these plots is listed in Table 2, which includes the Spearman rank order correlation coefficient with its associated null probability, the generalized Kendall's correlation coefficient for censored data and the Kendall's coefficient for partial correlation with censored data. One should note that, due to redshift effects, luminosity-luminosity plots will almost always show some correlation. Thus, we are primarily interested in the tightness of the correlations or the slopes. Furthermore, caution must be taken when applying statistical analysis to data sets that contain non-detections (upper limits), or "censored" data points. To deal with these problems we have used Astronomy SURVival analysis (**ASURV**) Rev 1.2 (Isobe & Feigelson 1990), which implement the methods presented in Isobe et al. (1986). We also used a test for partial correlation with censored data (Akritas & Siebert 1996) in order to excluded the redshift effect in the correlations.

In Figure 2 we show the distribution of the observed [Ne II], [Ne III], [Ne V], [O IV] and BAT luminosities (L_{BAT}) for our sample. The results of the Kolmogorov-Smirnov (K-S)

tests, comparing Seyfert 1s and 2s, for these quantities are listed in Table 3[2]. This table also includes information about the numbers of Seyfert 1 and Seyfert 2 galaxies, median values and standard deviations of the mean for the measured quantities. As is apparent from both the histograms and the K-S results, the two Seyfert types are statistically indistinguishable, i.e., there are essentially no differences between Seyfert 1s and 2s when we directly compare the BAT luminosities or any of the IR line strengths. This result is in agreement with the similar luminosities found for broad and narrow line sources, with optical Seyfert classifications, in the most recent study on the optical spectral properties of the BAT AGN (Winter et al. 2010). The similarity in observed IR properties between Seyfert types here is a strong indicator of the unique properties of the X-ray selected sample and the power of the X-ray selection technique to obtain as unbiased a sample as possible. The smallest null-test probability is for L_{BAT}, which, as we will discuss below, is evidence that Seyfert 2s suffer more from Compton scattering in the BAT band. Although there were too few of the "new BAT AGN" to separate them for a K-S on these quantities, the histograms indicate that they are relatively weaker in their observed emission line luminosities, compared to their BAT luminosities.

As mentioned before, a detailed statistical analysis for the different correlations between the BAT and mid-infrared luminosities is presented in Table 2. From this analysis the weaker correlation found in the [Ne II] - BAT relationship could be the result of active star formation contributing to the [Ne II] emission line in some of the AGN (e.g., Sturm et al. 2002; Schweitzer et al. 2006; Ho & Keto 2007; Meléndez et al. 2008b). On the other

[2]A probability value of less than 5% represents a high level of significance that two samples drawn from the same parent population would differ this much 5% of the time, i.e., that they are different. A strong level of significance is obtained for values smaller than 1% (e.g., Press et al. 1992; Bevington & Robinson 2003)

hand the better correlations are found between [Ne III], [Ne V] and [O IV] when compared to L_{BAT}, suggesting that, on average, there is no enhancement due to star formation contamination in the [Ne III] and [O IV] emission in the BAT sample. In Table 4 we present the linear regression fits for all this correlations. The somewhat steeper slopes for the Seyfert 2s are consistent with uncorrected for Compton scatter X-ray emission in the BAT band. The strong similarities between Seyfert types lessen when we compare the *ratios* of mid-IR line strengths and the X-ray continuum strength. In Figure 3, we show the ratios of L_{BAT} and [Ne II], [Ne III], and [Ne V] 14.32 μm compared to L_{BAT}/[O IV]. Of particular interest in this comparison is that below $\log L_{BAT}/[O\ IV] <\sim 2.0$ there are only two Seyfert 1 galaxies but thirteen Seyfert 2 galaxies ($\sim$ 40% of the Seyfert 2 population in our sample). Therefore, in these plots, one can see that the Seyfert 2s have lower ratios of L_{BAT} to the emission lines compared to the Seyfert 1s, which is, again, the effect of Compton scattering in the BAT band in the former. This result is in agreement with the K-S test null probability for this ratio, see Table 3. Similarly, there is only one Seyfert 2 galaxy with $\log L_{BAT}/[O\ IV] >\sim 3.0$. From the L_{BAT}/[O IV], the most extreme cases to study the effects of Compton scattering in the BAT band are: NGC 1365, NGC 2992, NGC 3281, NGC 7582, MRK 3 and MCG-03-34-064. By looking at the BAT data (Mushotzky et al. 2010, in preparation), MRK 3 has a flat spectrum with a photoelectric cutoff, consistent with a high column density but not a Compton thick absorber. On the other hand, NGC 1365, NGC 3281 and NGC 7582 are most probably Compton thick sources and the BAT data for NGC 2992 and MCG-03-34-064 have a low S/N which makes it difficult to constraint the spectrum well. These results suggest that the low BAT to [O IV] ratio is a marker for very high column densities towards the X-ray source, in agreement with previous studies (Meléndez et al. 2008a; Rigby et al. 2009; La Massa et al. 2009). These results argue in favor of the unified model of active galaxies, where the amount of X-ray emission suppressed, relative to an isotropic indicator for the AGN power, is related with the

absorbing column density towards the X-ray source (see also Bassani et al. 1999; Heckman et al. 2005; Netzer et al. 2006). The very tight correlation between the L_{BAT}/[O IV] and L_{BAT}/[Ne V] 14.32μm ratio also suggests that the latter can also be use as an excellent tracer for high X-ray column densities, specially when using the [Ne V] 24.32μm emission, which is less affected by dust extinction. The histograms for the ratios of L_{BAT} and [Ne II], [Ne III], and [Ne V] 14.32 μm are presented in Figure 4.

In Figure 5 we plot both the flux and luminosity of [Ne II], [Ne III] and [O IV] against those of [Ne V] 14.32μm. The very tight correlation between [Ne V] and [O IV] suggest that both of these lines are produced by the same physical process, i.e. photoionization by the AGN continuum (see also, Meléndez et al. 2008a,b). This is also true for the tight correlation between [Ne V] and [Ne III] found in our sample. While there is some scatter for [Ne III] which may also be due to star formation (Ho & Keto 2007), the tightness of the correlation suggests that [Ne III] is primarily produced by the AGN (see also Gorjian et al. 2007; Goulding & Alexander 2009), in agreement with the good correlation found between the [Ne III] and BAT luminosity. Furthermore, the tightness of these correlations, specially in flux-flux, suggests that the constant mid-infrared ratios observed are not dominated by aperture effects. This is due to the fact that the extraction aperture for the [O IV] is bigger than that for the [Ne III] and [Ne V]14μm, implying that the emitting regions where these lines originate are well within the central kpc of these sources, also in agreement with our previous photoionization studies (e.g., Meléndez et al. 2008a,b). Moreover, we found that all of the correlations presented, e.g., between the mid-infrared lines and the BAT luminosities, are not driven by distances effects as shown by the partial correlation analysis (see Table 2). Finally, the largest scatter occurs for [Ne II], which is consistent with the interpretation that this line may contains a significant contribution from stellar processes, as also evident in Figure 3. Note, however, that the correlation between [Ne II] and [Ne V] (see Table 2) is still strong, which is evidence that, on average, the observed [Ne II] emission in the BAT

sample is dominated by the AGN. From these results we will explore the range in elemental abundances for Neon and Oxygen, and the shape of the ionizing continuum in the 40 – 100 eV range among the BAT AGN in a follow-up study (M. Meléndez et al., in preparation).

The ratios of high-ionization lines to low-ionization lines can reveal the relative contributions of the AGN and star formation. In Figure 6, we show the ratios of [Ne III]/[Ne II] and [Ne V]14mum/[Ne II] compared to [O IV]/[Ne II] for the BAT sample. One result, which was also discussed in Meléndez et al. (2008b), is that the majority of our AGN have [Ne III]/[Ne II] greater than unity. This suggests that the AGN component in the mid-infrared emission lines is dominant in the BAT targets. These results are in agreement with the high-resolution *Spitzer* analysis of the 12μm sample by Tommasin et al. (2008) where they found the same range for the [Ne III]/[Ne II] and [O IV]/[Ne II] ratios. The tight correlation between [O IV] and [Ne V], also evident in Figure 3, is seen here as well. The [Ne V]/[Ne II] versus [O IV]/[Ne II] plot shows a number of sources, including several of the newly BAT-detected AGN and the two LINERs in the sample, with relatively weak high-ionization lines, which can result from a weak AGN, strong nuclear star formation, extinction towards the high-ionization region, or shielding of the NLR from the ionizing continuum. Comparing the [Ne III]/[Ne II] to the [Ne V]/[Ne II] we found the same overall trend, however, the slope of the former flattens towards lower ratios of [O IV]/[Ne II] possible due to the contribution of star formation to the [Ne III]. Interestingly, all these ratios are log normal distributed with a standard deviation of only ~ 0.3, except for the [Ne V]/[O IV] with a standard deviation of ~ 0.2. The [O IV]/[Ne II] emission line ratio was also compared with the redshift (z) in order to check if our previous results are been affected by aperture affects and found that the Spearman rank, $\rho_s = 0.129$; $P_\rho = 0.30$, and Kendall test, $\tau = 0.08$;$P_\tau = 0.27$, did not show any correlation with z. A similar result was obtained for the [O IV]/[Ne III] ratios and the redshift where we found no correlation, with a Spearman rank, $\rho_s = -0.05$; $P_\rho = 0.66$, and Kendall test, $\tau = -0.05$;$P_\tau = 0.51$.

3.2. Extinction in the mid-IR

If wavelength-dependent extinction is important in the mid-IR, it should be evident when comparing the strengths of [Ne V] 14.32μm and [Ne V] 24.32μm. Dudik et al. (2007) calculated the theoretical values of this ratio as a function of density and electron temperature (see their Fig. 1). As density increases, the 24.32μm line is suppressed relative to the 14.32μm line, hence the most likely way in which the ratio can fall below the theoretical low-density limit is extinction, suggesting that it should be stronger for the shorter-wavelength line. In Figure 7, we show the correlation between the two [Ne V] lines for the BAT sample, with the theoretical low-density limit over-plotted. We note that the correlation between the [Ne V] emission lines is strong and is similar in both flux and luminosities, meaning that there is a true linear correlation, see Table 4.

Five out of six of the newly BAT-detected AGN have ratios below the low density limit, indicating possible dust extinction. In Figure 8, we compared the [Ne V] line ratio to the host galaxy inclination[3]. Moreover, all of the newly BAT-detected AGN are found on inclined host galaxies which argues in favor of an scenario where the optical signatures of the AGN may been missed in this group of newly BAT-detected AGN due to extinction in the plane of the host galaxy; as suggested by Kirhakos & Steiner (1990) and Simcoe et al. (1997) and more recently by GA09. However, one must note from Figure 8, that there is no correlation between the [Ne V] line ratio and the host galaxy inclination. Hence, host galaxy inclination cannot be solely responsible for the observed mid-infrared extinction in our sample.

In addition to providing some insight into the nature of the newly BAT-detected AGN,

[3]The values for the major and minor diameter of the host galaxy, a and b respectively, were taken from NED

these plots show that $\sim$ 40% of the full sample show some evidence for dust extinction. This result is in good agreement with the percentage of Seyfert galaxies that falls below the neon ratio low-density limit from the most recent high-resolution spectroscopy of the 12μm sample (Tommasin et al. 2010). If extinction were responsible, it is plausible that the tightness of the [Ne III]- L_{BAT} correlation may be due to the combined effects of mid-IR extinction and X-ray decrement due to Compton scatter in the BAT band. Similarly, the larger scatter for [O IV]- L_{BAT} may be due, in part, to the lower extinction for [O IV], compared to [Ne III], hence the variations in the observed X-ray, due to different column densities toward the nuclear region, become the dominant effect.

4. Comparison between BAT AGN and other Sources

Following the mid-infrared properties for the BAT AGN sample we investigated the relationship between different types of galaxies in light of new mid-infrared diagnostics. For comparison we searched the literature for the most recent *Spitzer* high-resolution IRS spectroscopy, from this we used the volume-limited sample of bolometrically luminous galaxies ($L_{IR} > 3 \times 10^9 L_\odot$) to a distance of $D < 15$ Mpc of GA09 which includes H II galaxies, LINERS, optically classified AGN and optically unclassified galaxies. We also used the recent atlas of starburst galaxies by B09 that includes starburst galaxies with and without evidence of an AGN. Finally, we used a sample of extreme starburst galaxies which includes blue compact dwarfs (BCD) from H09. When a source was present in more than one compilation we gave priority to the data analysis and extraction presented in this work, followed by GA09. Given the high ionization potential for Ne^{+4}, the mid-infrared [Ne V] emission lines are claimed to be an unambiguous signatures of an AGN (e.g., Satyapal et al. 2007, 2009). In this regard, using [Ne V] 14.32μm, GA09 identified AGN activity in sources that were previously unclassified by their optical spectra. Moreover, while theoretical

models predict that some fraction of [Ne V] can be produce by energetic starbursts (e.g., Abel & Satyapal 2008), H09 did not detect [Ne V] emission in their sample of extreme starburst galaxies.

However, some problems arise when looking at the [Ne V] emission in AGN. In our sample, [Ne V] 14.32μm and 24.32μm were not detected in $\sim$ 10% and $\sim$ 15% of the sources, respectively. Similar results are obtained for the [Ne V] 14.32μm and 24.32μm in the *Spitzer* high-resolution spectroscopy of the 12μm Seyfert galaxies (Tommasin et al. 2008, 2010). This suggests that because of dust extinction and instrumental sensitivity, [Ne V] emission could go undetected even in strong AGN. On the other hand, [Ne II], [Ne III] and [O IV] are present in AGN, BCD, starburst, H II galaxies and have a wide range of ionization potentials and critical densities which allow us to study the connection between the active nucleus and star formation. One must note that H09 found that the most likely contributor to the [O IV] emission in starburst and BCD galaxies are Wolf-Rayet stars. In this regard, and despite the fact that [O IV] emission traces the AGN intrinsic luminosity in *pre-selected* AGN, [O IV] cannot be solely associated with the power of the AGN.

In Figure 9 we compare the [Ne III]/[Ne II] versus [O IV]/[Ne III] ratios. From this comparison there are four distinctive regions to note: 1) the BAT AGN branch; 2) below the BAT AGN are the starburst (SB) and HII galaxies which have an apparent [Ne II] excess; 3) above the BAT AGN are the BCD and two WR galaxies from GA09 (II Zw40 and NGC 1569), and 4) LINERs, which seem to follow a connecting path between AGN and SB/HII galaxies but are mainly found in the lower-luminosity region of the BAT AGN. Despite the fact that [O IV] has been detected in BCD, SB and HII galaxies, WR and BCD galaxies cannot produce [O IV] as effectively as [Ne III], unlike in AGN, making these sources have relative low [O IV]/[Ne III] ratios. From this diagram we found that LINERs are consistent with the BAT AGN branch. There is also a small "merge" region, at the

lower end of the BAT AGN branch, that comprises LINERs and starburst galaxies with evidence for an AGN. In this region we found five of the [Ne V] AGN from GA09, some of which don't have optical signatures for an AGN. Among the [Ne V] AGN, NGC 660 and NGC 3628 have shown some evidence to harbor a LINER (Filho et al. 2004; Dudik et al. 2005; Flohic et al. 2006). Also, based on this diagnostic, we found that NGC 520, NGC 4676 and NGC 1614 could harbor an AGN, although these starburst galaxies don't show optical evidence of such (B09). In this regard, there is X-ray evidence for a Compton thick AGN in NGC 1614 (Risaliti et al. 2000), in agreement with our diagnostic. Interestingly, these possible AGN are found in interacting systems or mergers with strong star formation. Perhaps, interacting or merger systems may provide enough fuel to the nuclear regions of the galaxy to trigger both the nuclear star formation and the AGN. One must note that most of the non-BAT AGNs, e.g., the SB+AGN sources from B09 and [Ne V] 14.32μm-AGN (GA09) have smaller mid-infrared ratios than that found for the BAT AGN. From this we found that most of the BAT AGNs have [Ne III]/[Ne II] and [O IV]/[Ne III] ratios bigger than unity, contrary to those of non-BAT AGNs presented in this study, e.g., AGN that have been selected because their optical and mid-infrared emission line signatures. This result suggest that the BAT sample represents a unique opportunity to study the most "pure" AGN, i.e., sources in which their optical/mid-infrared emission signatures are dominated by the AGN. One must note from Figure 9 that the [Ne III]/[Ne II] ratio as a stand alone diagnostic may overestimate the fraction of AGN because Wolf-Rayet stars or another energetic phenomena (perhaps ULXs) could produce [Ne III]/[Ne II] ratios even higher than those found on the BAT AGN. However, by further constraining this ratio by using [O IV] we were able to separate AGN from energetic starbursts and other sources.

As we mentioned before, caution must be taken when comparing fluxes between *Spitzer* High-Resolution orders because of the differences in size. However, given the similarities between the ionization potentials for [Ne III] and [O IV], it is likely that both lines originate

in similar regions, thus introducing less uncertainty in the use of the [O IV]/[Ne III] ratio. Nevertheless, in HII/SB/BCD galaxies we could be underestimating the amount of [Ne III] that is associated with the same physical conditions that produce [O IV], e.g., WR stars. This will cause this ratio, when derived from equal apertures extractions, to be displaced toward even smaller values thus, enhancing the differences between these sources and our sample of hard X-ray selected AGN.

5. Conclusions

Using *Spitzer* high-resolution IRS spectra, we have examined the mid-IR emission-line properties of a sample of hard X-ray selected AGN, detected by *Swift*/BAT. Our principle conclusions are as follows.

1. The luminosity distribution for the mid-infrared emission lines and BAT continuum luminosities show no differences between Seyfert 1 and Seyfert 2 populations for the BAT sample. The correlations between all the mid-infrared emission lines and BAT luminosities are statistically significant even when factoring the distance effect in luminosity-luminosity correlations. The dispersion/tightness in these correlations is due to differences in the X-ray absorbing column densities, dust extinction and/or nuclear star formation activity. Moreover, the tight correlation found in the [Ne III]-BAT relationship suggests that, on average, there is no enhancement due to star formation contamination in the [Ne III] emission in the BAT sample. Also, the slopes for the [Ne III],[Ne V] and [O IV] versus BAT luminosities relationships are smaller in Seyfert 1 galaxies than in Seyfert 2s (which are around unity), which suggests that, while the amount of extinction towards the NLR is similar in both types, the X-ray absorbing columns are large enough in Seyfert 2s to affect the hard X-ray band, confirming the results of Meléndez et al. (2008a) and Rigby et al. (2009). This results is in agreement with the fact that the BAT/[O IV] ratio statistically

separates Seyfert 1s and Seyfert 2s.

2. Although all of the correlations among the mid-infrared emission lines are strong, the worst correlations are for [Ne V]-[Ne II] and [O IV]-[Ne II], because of enhancement of the [Ne II] from nuclear stellar activity (see also Meléndez et al. 2008b). While the tightness of these mid-infrared correlations suggests that dust extinction is not the driving physical process behind the mid-infrared relationships, approximately ∼40% (including upper limits) of the sample have values for the ratio of the [Ne V] emission lines below the low-density theoretical limit, suggesting dust extinction as the physical process responsible. Exploring this, we found that all of the newly discovered BAT AGNs in our sample, which are under-luminous in [O IV] and [Ne V]14/24μm, are found on inclined host galaxies, and all but one have [Ne V] ratios below the critical density limit. Hence, it is likely that the newly found BAT AGN in our sample lack optical AGN signatures because of host galaxy extinction towards their NLRs. One must note that host galaxy inclination cannot be responsible for the observed extinction in all the BAT AGN sample.

3. We compared the BAT AGNs with different starburst and H II galaxies, so-called [Ne V] active galaxies, and LINERs (Goulding & Alexander 2009; Bernard-Salas et al. 2009; Hao et al. 2009). We found that the BAT AGN fall into a distinctive region based on the [Ne III]/[Ne II] and [O IV]/[Ne III] ratios. We found that using [Ne III] and [O IV] emission, previously connected with AGN power (e.g., Gorjian et al. 2007; Meléndez et al. 2008a), does not unambiguously identify AGNs as an stand along diagnostic because Wolf-Rayet stars or another energetic phenomena (perhaps ULXs) could enhance the observed emission. While it is likely that detection of [Ne V] indicates the presence of an AGN, the strongest of the [Ne V] lines have ∼1/3 less flux than [O IV] an thus will be more difficult to detect in weak or faint AGN. Therefore, our composite method using the strong [Ne II], [Ne III] and [O IV], represents a strong and simple diagnostic by using only three emission lines

to identify an AGN. Based on this diagnostic, we found that NGC 520, NGC 4676 and NGC 1614 could harbor an AGN, although these starburst galaxies don't show optical evidence of such (B09). In this regard, there is X-ray evidence for a Compton thick AGN in NGC 1614 (Risaliti et al. 2000), in agreement with our diagnostic.

We also found that most of the non-BAT AGNs presented in our study, AGN that have been selected because their optical and mid-infrared emission line signatures, have smaller mid-infrared ratios than that found for the BAT AGN. This result suggest that the BAT sample represents a unique opportunity to study the most "pure" AGN, sources in which their optical/mid-infrared emission signatures are dominated by the AGN. Therefore, providing the most unbiased sample in terms of galaxy population and stellar content.

This research was supported by an appointment to the NASA Postdoctoral Program at the Goddard Space Flight Center, administered by Oak Ridge Associated Universities through a contract with NASA. L.M.W. acknowledges support under Hubble Fellowship program number HST-HF-51263.01-A from the Space Telescope Science Institute, which is operated by the Association of Universities for Research in Astronomy, Incorporated, under NASA contract NAS5-26555. This research has made use of the NASA/IPAC Extragalactic Database (NED) which is operated by the Jet Propulsion Laboratory, California Institute of Technology, under contract with the National Aeronautics and Space Administration. The IRS was a collaborative venture between Cornell University and Ball Aerospace Corporation funded by NASA through the Jet Propulsion Laboratory and Ames Research Center. SMART was developed by the IRS Team at Cornell University and is available through the *Spitzer* Science Center at Caltech.

REFERENCES

Abel, N. P., & Satyapal, S. 2008, ApJ, 678, 686

Akritas, M. G., & Siebert, J. 1996, MNRAS, 278, 919

Armus, L., Bernard-Salas, J., Spoon, H. W. W., Marshall, J. A., Charmandaris, V., Higdon, S. J. U., Desai, V., Hao, L., Teplitz, H. I., Devost, D., Brandl, B. R., Soifer, B. T., & Houck, J. R. 2006, ApJ, 640, 204

Armus, L., Charmandaris, V., Bernard-Salas, J., Spoon, H. W. W., Marshall, J. A., Higdon, S. J. U., Desai, V., Teplitz, H. I., Hao, L., Devost, D., Brandl, B. R., Wu, Y., Sloan, G. C., Soifer, B. T., Houck, J. R., & Herter, T. L. 2007, ApJ, 656, 148

Barger, A. J., Cowie, L. L., Mushotzky, R. F., Yang, Y., Wang, W., Steffen, A. T., & Capak, P. 2005, AJ, 129, 578

Barmby, P., Alonso-Herrero, A., Donley, J. L., Egami, E., Fazio, G. G., Georgakakis, A., Huang, J., Laird, E. S., Miyazaki, S., Nandra, K., Park, S. Q., Pérez-González, P. G., Rieke, G. H., Rigby, J. R., & Willner, S. P. 2006, ApJ, 642, 126

Bassani, L., Dadina, M., Maiolino, R., Salvati, M., Risaliti, G., della Ceca, R., Matt, G., & Zamorani, G. 1999, ApJS, 121, 473

Bernard-Salas, J., Spoon, H. W. W., Charmandaris, V., Lebouteiller, V., Farrah, D., Devost, D., Brandl, B. R., Wu, Y., Armus, L., Hao, L., Sloan, G. C., Weedman, D., & Houck, J. R. 2009, ApJS, 184, 230

Bevington, P. R., & Robinson, D. K. 2003, Data reduction and error analysis for the physical sciences, ed. P. R. Bevington & D. K. Robinson

Crenshaw, D. M., & Kraemer, S. B. 2000, ApJ, 532, L101

Dale, D. A., Smith, J. D. T., Armus, L., Buckalew, B. A., Helou, G., Kennicutt, Jr., R. C., Moustakas, J., Roussel, H., Sheth, K., Bendo, G. J., Calzetti, D., Draine, B. T., Engelbracht, C. W., Gordon, K. D., Hollenbach, D. J., Jarrett, T. H., Kewley, L. J., Leitherer, C., Li, A., Malhotra, S., Murphy, E. J., & Walter, F. 2006, ApJ, 646, 161

Diamond-Stanic, A. M., Rieke, G. H., & Rigby, J. R. 2009, ApJ, 698, 623

Dudik, R. P., Satyapal, S., Gliozzi, M., & Sambruna, R. M. 2005, ApJ, 620, 113

Dudik, R. P., Satyapal, S., & Marcu, D. 2009, ApJ, 691, 1501

Dudik, R. P., Weingartner, J. C., Satyapal, S., Fischer, J., Dudley, C. C., & O'Halloran, B. 2007, ApJ, 664, 71

Farrah, D., Bernard-Salas, J., Spoon, H. W. W., Soifer, B. T., Armus, L., Brandl, B., Charmandaris, V., Desai, V., Higdon, S., Devost, D., & Houck, J. 2007, ApJ, 667, 149

Filho, M. E., Fraternali, F., Markoff, S., Nagar, N. M., Barthel, P. D., Ho, L. C., & Yuan, F. 2004, A&A, 418, 429

Flohic, H. M. L. G., Eracleous, M., Chartas, G., Shields, J. C., & Moran, E. C. 2006, ApJ, 647, 140

Franceschini, A., Manners, J., Polletta, M. d. C., Lonsdale, C., Gonzalez-Solares, E., Surace, J., Shupe, D., Fang, F., Xu, C. K., Farrah, D., Berta, S., Rodighiero, G., Perez-Fournon, I., Hatziminaoglou, E., Smith, H. E., Siana, B., Rowan-Robinson, M., Nandra, K., Babbedge, T., Vaccari, M., Oliver, S., Wilkes, B., Owen, F., Padgett, D., Frayer, D., Jarrett, T., Masci, F., Stacey, G., Almaini, O., McMahon, R., Johnson, O., Lawrence, A., & Willott, C. 2005, AJ, 129, 2074

Genzel, R., Lutz, D., Sturm, E., Egami, E., Kunze, D., Moorwood, A. F. M., Rigopoulou, D., Spoon, H. W. W., Sternberg, A., Tacconi-Garman, L. E., Tacconi, L., & Thatte, N. 1998, ApJ, 498, 579

George, I. M., Turner, T. J., Netzer, H., Nandra, K., Mushotzky, R. F., & Yaqoob, T. 1998, ApJS, 114, 73

Gorjian, V., Cleary, K., Werner, M. W., & Lawrence, C. R. 2007, ApJ, 655, L73

Goulding, A. D., & Alexander, D. M. 2009, MNRAS, 398, 1165

Hao, L., Wu, Y., Charmandaris, V., Spoon, H. W. W., Bernard-Salas, J., Devost, D., Lebouteiller, V., & Houck, J. R. 2009, ApJ, 704, 1159

Heckman, T. M., Kauffmann, G., Brinchmann, J., Charlot, S., Tremonti, C., & White, S. D. M. 2004, ApJ, 613, 109

Heckman, T. M., Ptak, A., Hornschemeier, A., & Kauffmann, G. 2005, ApJ, 634, 161

Higdon, S. J. U., Devost, D., Higdon, J. L., Brandl, B. R., Houck, J. R., Hall, P., Barry, D., Charmandaris, V., Smith, J. D. T., Sloan, G. C., & Green, J. 2004, PASP, 116, 975

Ho, L. C., & Keto, E. 2007, ApJ, 658, 314

Isobe, T., & Feigelson, E. D. 1990, in Bulletin of the American Astronomical Society, Vol. 22, Bulletin of the American Astronomical Society, 917–918

Isobe, T., Feigelson, E. D., Akritas, M. G., & Babu, G. J. 1990, ApJ, 364, 104

Isobe, T., Feigelson, E. D., & Nelson, P. I. 1986, ApJ, 306, 490

Kessler, M. F., Steinz, J. A., Anderegg, M. E., Clavel, J., Drechsel, G., Estaria, P., Faelker, J., Riedinger, J. R., Robson, A., Taylor, B. G., & Ximénez de Ferrán, S. 1996, A&A, 315, L27

Kirhakos, S. D., & Steiner, J. E. 1990, AJ, 99, 1722

Koratkar, A., & Blaes, O. 1999, PASP, 111, 1

Kuraszkiewicz, J. K., Wilkes, B. J., Hooper, E. J., McLeod, K. K., Wood, K., Bjorkman, J., Delain, K. M., Hughes, D. H., Elvis, M. S., Impey, C. D., Lonsdale, C. J., Malkan, M. A., McDowell, J. C., & Whitney, B. 2003, ApJ, 590, 128

La Massa, S. M., Heckman, T. M., Ptak, A., Hornschemeier, A., Martins, L., Sonnentrucker, P., & Tremonti, C. 2009, ApJ, 705, 568

Landi, R., Masetti, N., Morelli, L., Palazzi, E., Bassani, L., Malizia, A., Bazzano, A., Bird, A. J., Dean, A. J., Galaz, G., Minniti, D., & Ubertini, P. 2007, ApJ, 669, 109

Levine, A. M., Lang, F. L., Lewin, W. H. G., Primini, F. A., Dobson, C. A., Doty, J. P., Hoffman, J. A., Howe, S. K., Scheepmaker, A., Wheaton, W. A., Matteson, J. L., Baity, W. A., Gruber, D. E., Knight, F. K., Nolan, P. L., Pelling, R. M., Rothschild, R. E., & Peterson, L. E. 1984, ApJS, 54, 581

Lutz, D., Maiolino, R., Spoon, H. W. W., & Moorwood, A. F. M. 2004, A&A, 418, 465

Lutz, D., Yan, L., Armus, L., Helou, G., Tacconi, L. J., Genzel, R., & Baker, A. J. 2005, ApJ, 632, L13

Markwardt, C. B., Tueller, J., Skinner, G. K., Gehrels, N., Barthelmy, S. D., & Mushotzky, R. F. 2005, ApJ, 633, L77

Masetti, N., Mason, E., Morelli, L., Cellone, S. A., McBride, V. A., Palazzi, E., Bassani, L., Bazzano, A., Bird, A. J., Charles, P. A., Dean, A. J., Galaz, G., Gehrels, N., Landi, R., Malizia, A., Minniti, D., Panessa, F., Romero, G. E., Stephen, J. B., Ubertini, P., & Walter, R. 2008, A&A, 482, 113

Matt, G. 2000, A&A, 355, L31

Meléndez, M., Kraemer, S. B., Armentrout, B. K., Deo, R. P., Crenshaw, D. M., Schmitt, H. R., Mushotzky, R. F., Tueller, J., Markwardt, C. B., & Winter, L. 2008a, ApJ, 682, 94

Meléndez, M., Kraemer, S. B., Schmitt, H. R., Crenshaw, D. M., Deo, R. P., Mushotzky, R. F., & Bruhweiler, F. C. 2008b, ApJ, 689, 95

Mulchaey, J. S., Koratkar, A., Ward, M. J., Wilson, A. S., Whittle, M., Antonucci, R. R. J., Kinney, A. L., & Hurt, T. 1994, ApJ, 436, 586

Mushotzky, R. 2004, in Astrophysics and Space Science Library, Vol. 308, Supermassive Black Holes in the Distant Universe, ed. A. J. Barger, 53–+

Netzer, H., Mainieri, V., Rosati, P., & Trakhtenbrot, B. 2006, A&A, 453, 525

Peterson, B. M., Ferrarese, L., Gilbert, K. M., Kaspi, S., Malkan, M. A., Maoz, D., Merritt, D., Netzer, H., Onken, C. A., Pogge, R. W., Vestergaard, M., & Wandel, A. 2004, ApJ, 613, 682

Press, W. H., Teukolsky, S. A., Vetterling, W. T., & Flannery, B. P. 1992, Numerical recipes in FORTRAN. The art of scientific computing, ed. T. S. A. V. W. T. . F. B. P. Press, W. H.

Rigby, J. R., Diamond-Stanic, A. M., & Aniano, G. 2009, ApJ, 700, 1878

Risaliti, G., Gilli, R., Maiolino, R., & Salvati, M. 2000, A&A, 357, 13

Satyapal, S., Böker, T., Mcalpine, W., Gliozzi, M., Abel, N. P., & Heckman, T. 2009, ApJ, 704, 439

Satyapal, S., Sambruna, R. M., & Dudik, R. P. 2004, A&A, 414, 825

Satyapal, S., Vega, D., Heckman, T., O'Halloran, B., & Dudik, R. 2007, ApJ, 663, L9

Schmitt, H. R., Donley, J. L., Antonucci, R. R. J., Hutchings, J. B., & Kinney, A. L. 2003, ApJS, 148, 327

Schweitzer, M., Lutz, D., Sturm, E., Contursi, A., Tacconi, L. J., Lehnert, M. D., Dasyra, K. M., Genzel, R., Veilleux, S., Rupke, D., Kim, D., Baker, A. J., Netzer, H., Sternberg, A., Mazzarella, J., & Lord, S. 2006, ApJ, 649, 79

Simcoe, R., McLeod, K. K., Schachter, J., & Elvis, M. 1997, ApJ, 489, 615

Sturm, E., Lutz, D., Verma, A., Netzer, H., Sternberg, A., Moorwood, A. F. M., Oliva, E., & Genzel, R. 2002, A&A, 393, 821

Tommasin, S., Spinoglio, L., Malkan, M. A., & Fazio, G. 2010, ApJ, 709, 1257

Tommasin, S., Spinoglio, L., Malkan, M. A., Smith, H., González-Alfonso, E., & Charmandaris, V. 2008, ApJ, 676, 836

Tueller, J., Baumgartner, W. H., Markwardt, C. B., Skinner, G. K., Mushotzky, R. F., Ajello, M., Barthelmy, S., Beardmore, A., Brandt, W. N., Burrows, D., Chincarini, G., Campana, S., Cummings, J., Cusumano, G., Evans, P., Fenimore, E., Gehrels, N., Godet, O., Grupe, D., Holland, S., Kennea, J., Krimm, H. A., Koss, M., Moretti, A., Mukai, K., Osborne, J. P., Okajima, T., Pagani, C., Page, K., Palmer, D., Parsons, A., Schneider, D. P., Sakamoto, T., Sambruna, R., Sato, G., Stamatikos, M., Stroh, M., Ukwatta, T. N., & Winter, L. 2009, ArXiv e-prints

Tueller, J., Mushotzky, R. F., Barthelmy, S., Cannizzo, J. K., Gehrels, N., Markwardt, C. B., Skinner, G. K., & Winter, L. M. 2008, ApJ, 681, 113

Ueda, Y., Eguchi, S., Terashima, Y., Mushotzky, R., Tueller, J., Markwardt, C., Gehrels, N., Hashimoto, Y., & Potter, S. 2007, ApJ, 664, L79

Véron-Cetty, M., & Véron, P. 2006, A&A, 455, 773

Weedman, D. W., Hao, L., Higdon, S. J. U., Devost, D., Wu, Y., Charmandaris, V., Brandl, B., Bass, E., & Houck, J. R. 2005, ApJ, 633, 706

Werner, M. W., Roellig, T. L., Low, F. J., Rieke, G. H., Rieke, M., Hoffmann, W. F., Young, E., Houck, J. R., Brandl, B., Fazio, G. G., Hora, J. L., Gehrz, R. D., Helou, G., Soifer, B. T., Stauffer, J., Keene, J., Eisenhardt, P., Gallagher, D., Gautier, T. N., Irace, W., Lawrence, C. R., Simmons, L., Van Cleve, J. E., Jura, M., Wright, E. L., & Cruikshank, D. P. 2004, ApJS, 154, 1

Winter, L. M., Lewis, K. T., Koss, M., Veilleux, S., Keeney, B., & Mushotzky, R. F. 2010, ApJ, 710, 503

Winter, L. M., Mushotzky, R. F., Reynolds, C. S., & Tueller, J. 2009a, ApJ, 690, 1322

Winter, L. M., Mushotzky, R. F., Terashima, Y., & Ueda, Y. 2009b, ApJ, 701, 1644

Winter, L. M., Mushotzky, R. F., Tueller, J., & Markwardt, C. 2008, ApJ, 674, 686

This manuscript was prepared with the AAS LaTeX macros v5.2.

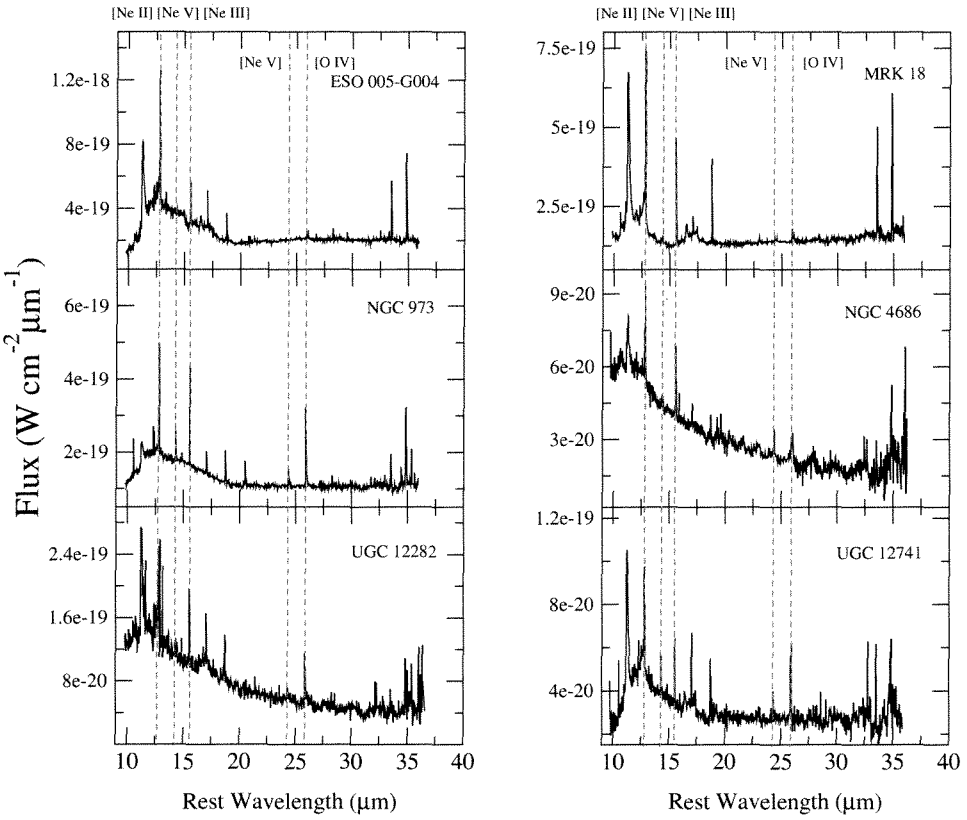

Fig. 1.— Combined *Spitzer* IRS SH and LH spectra for the newly detected AGN in the BAT sample. The [Ne II] 12.81 μm, [Ne III] 15.56 μm, [Ne V] 14.32 μm, [Ne V] 24.32 μm, and [O IV] 25.89 μm lines are indicated by the vertical lines. Note the drop in flux at $\lambda \lesssim 12\mu$m, particularly for ESO 005-G004, NGC 973, and UGC 12741, due to absorption by silicate grains. The strong emission line features at ~33 μm and ~35 μm correspond to [S III] and [Si II], respectively.

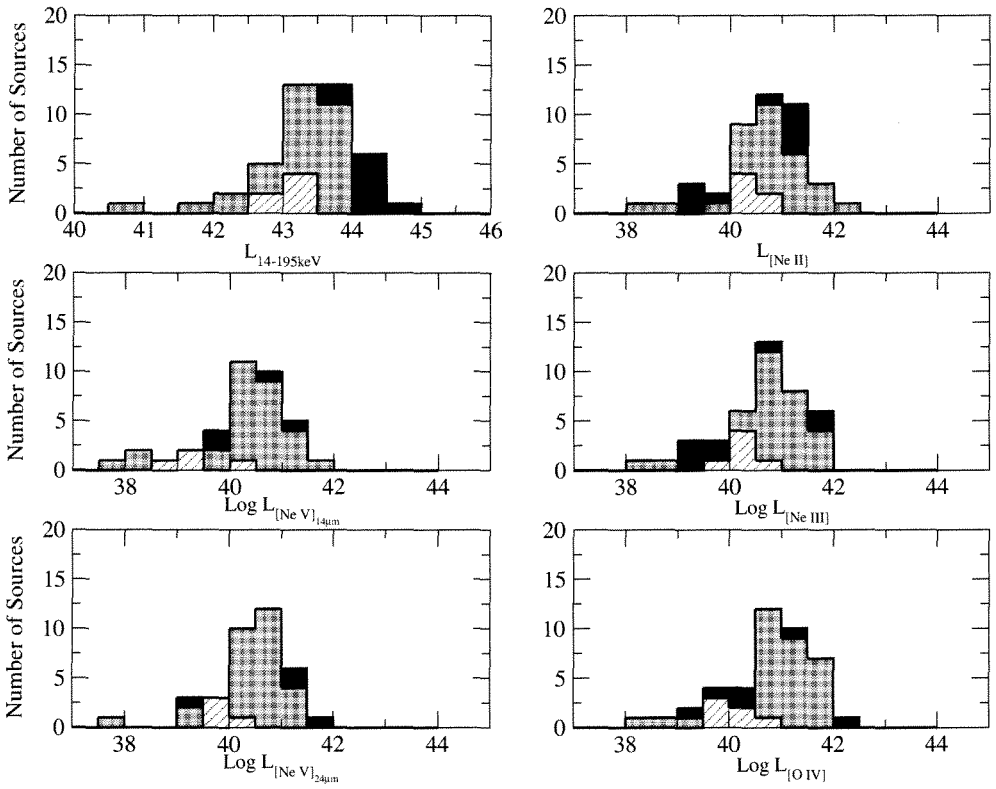

Fig. 2.— Histograms for the mid-infrared and BAT (14- 195 keV) luminosities for our sample. Seyfert 1 and Seyfert 2 galaxies are indicated with solid black and gray bins, respectively. The newly detected BAT AGN are indicated in bins with dashed lines; note that their [Ne III] and [O IV] luminosities appear to be low, i.e., compared to AGN with similar BAT luminosities. The K-S test for these emission line luminosities show that two samples drawn from the same population would differ this much $\sim$ 18.1%, $\sim$ 96.6%, $\sim$ 98.4%, $\sim$ 98.7%, $\sim$ 40.2% and $\sim$ 86.4% of the time for the BAT, [Ne II], [Ne V] 14μm, [Ne III], [Ne V] 24μm and [O IV] luminosity distributions, respectively.

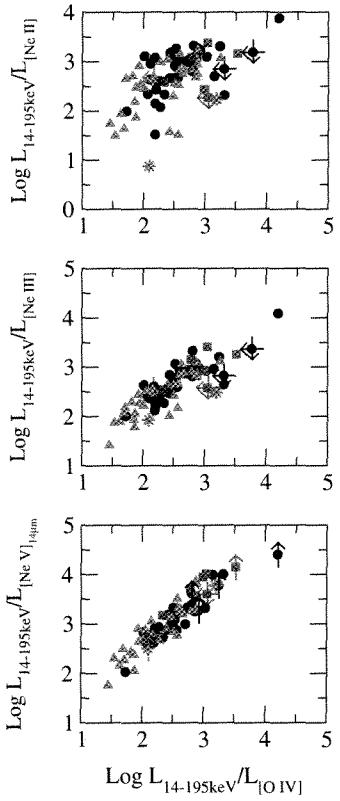

Fig. 3.— Comparison between the ratios of the BAT band and the mid-infrared emission lines. Seyfert 1 galaxies are presented as black circles, Seyfert 2 galaxies are red triangles, blue squares represent the newly detected BAT AGN and green stars are LINERs. Of particular interest is the statistically significant (see Table 3) separation between Seyfert types in the $L_{14-195keV}/L_{[O\ IV]}$ ratio, in agreement with this ratio being an indicator of Compton scattering in the BAT band. Of particular interest in this comparison is that below $L_{BAT}/[O\ IV] <\sim 2.0$ there are only two Seyfert 1 galaxies but thirteen Seyfert 2 galaxies ($\sim 40\%$ of the Seyfert 2 population)

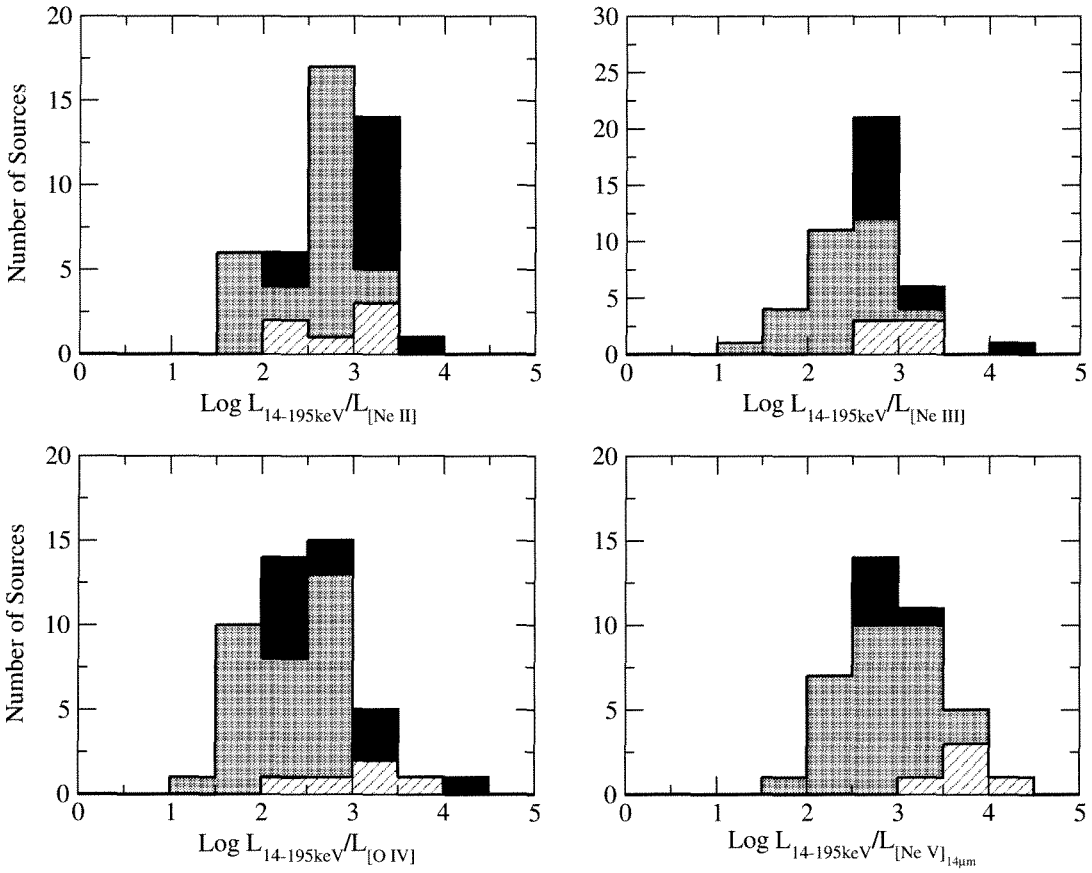

Fig. 4.— Histograms for the ratios of the BAT band and the mid-infrared emission lines. Seyfert 1 and Seyfert 2 galaxies are indicated with solid black and gray bins, respectively. The newly detected BAT AGN are indicated in bins with dashed lines. Interestingly, all these ratios are log normal distributed with a standard deviation of only 0.5, except for the $L_{14-195keV}/L_{[NeIII]}$ with a standard deviation of 0.4. The K-S test for these ratios show that two samples drawn from the same population would differ this much $\sim 2.8\%$, $\sim 9.0\%$, $\sim 2.4\%$, $\sim 26.1\%$ of the time for the $L_{14-195keV}/L_{[Ne\ II]}$, $L_{14-195keV}/L_{[Ne\ III]}$, $L_{14-195keV}/L_{[O\ IV]}$ and $L_{14-195keV}/L_{[Ne\ V](14\mu m)}$ distributions, respectively.

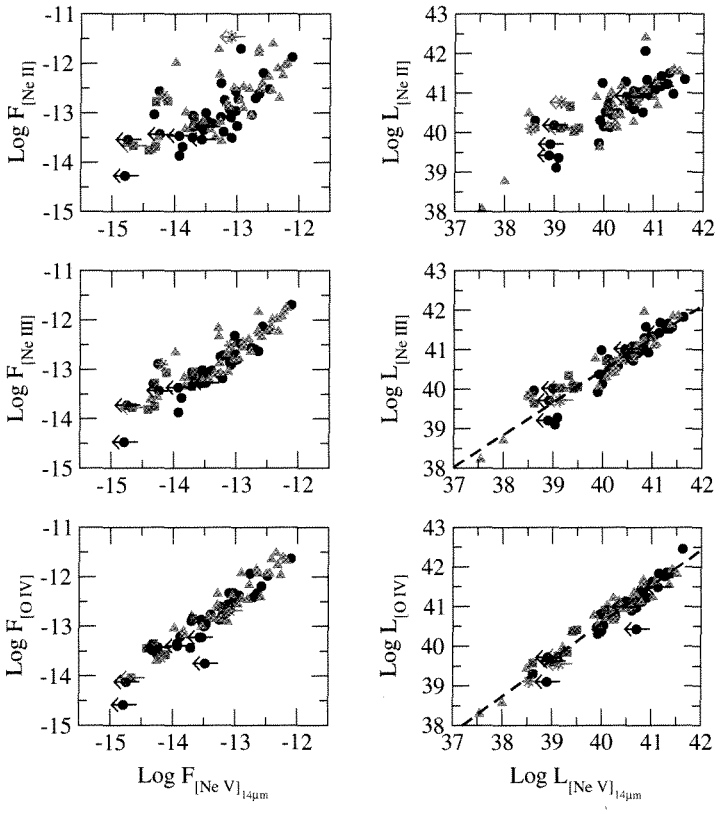

Fig. 5.— Correlation between [Ne II],[Ne III], [Ne V]14μm and [O IV] fluxes and luminosities. Symbols are the same as in Figure 3. The dashed line represents the linear regression for the full sample (see Table 4). The tightness of the correlation between [Ne V] and [O IV] suggests both a narrow range in elemental abundances and similar ionizing continua among the BAT AGN.

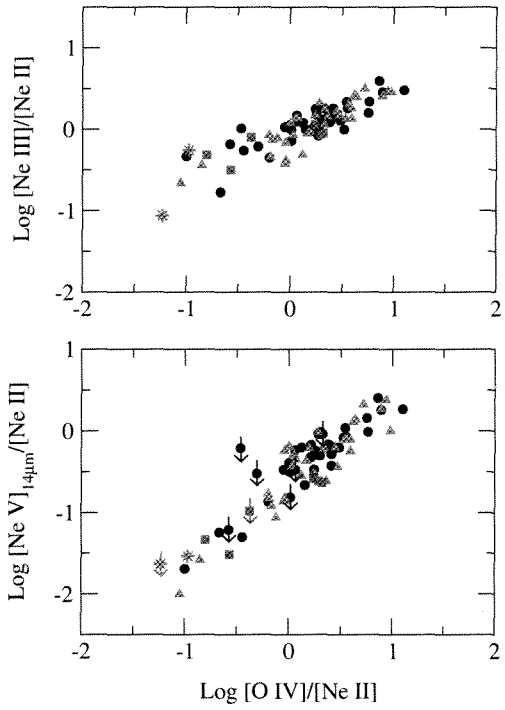

Fig. 6.— [Ne III]/[Ne II] and [Ne V]14μm/[Ne II] versus [O IV]/[Ne II] ratios for Seyfert 1, Seyfert 2, BAT-detected AGNs and LINERs in the BAT sample. The majority of the objects have [Ne III]/[Ne II] > 1, which has been shown to be typical of AGN-ionized emission-line gas (e.g., Meléndez et al. 2008b). The the [Ne V] and [O IV] ratios appear well-correlated, as expected given the tight correlation seen in Figure 5.

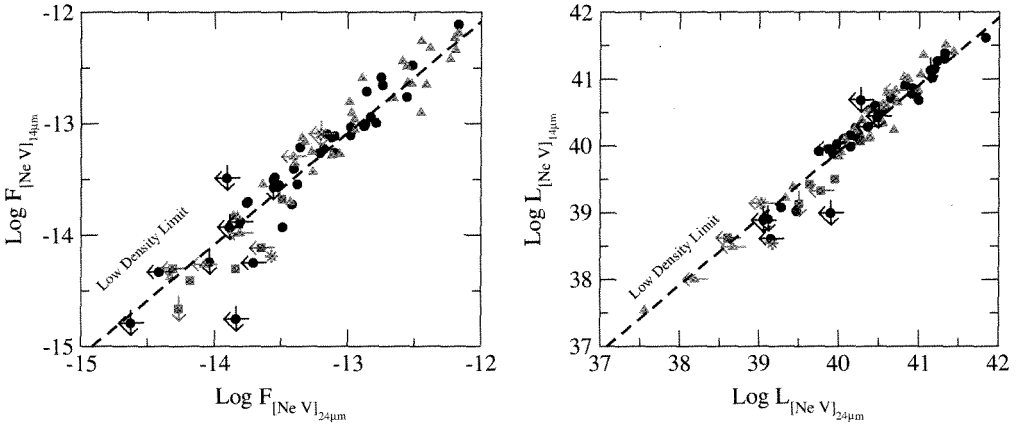

Fig. 7.— Correlation between the [NeV]24.32μm and [NeV]14.32μm fluxes and luminosities for our X-ray selected sample. The low-density limit for this ratio is given by the dashed line; AGN lying below and to the right have [NeV]14.32μm/[NeV]24.32μm ratios greater than the theoretical limit (Dudik et al. 2007). The majority of the newly-detected BAT AGN have ratios below the limit, implying dust extinction towards the [NeV]14μm emitting region.

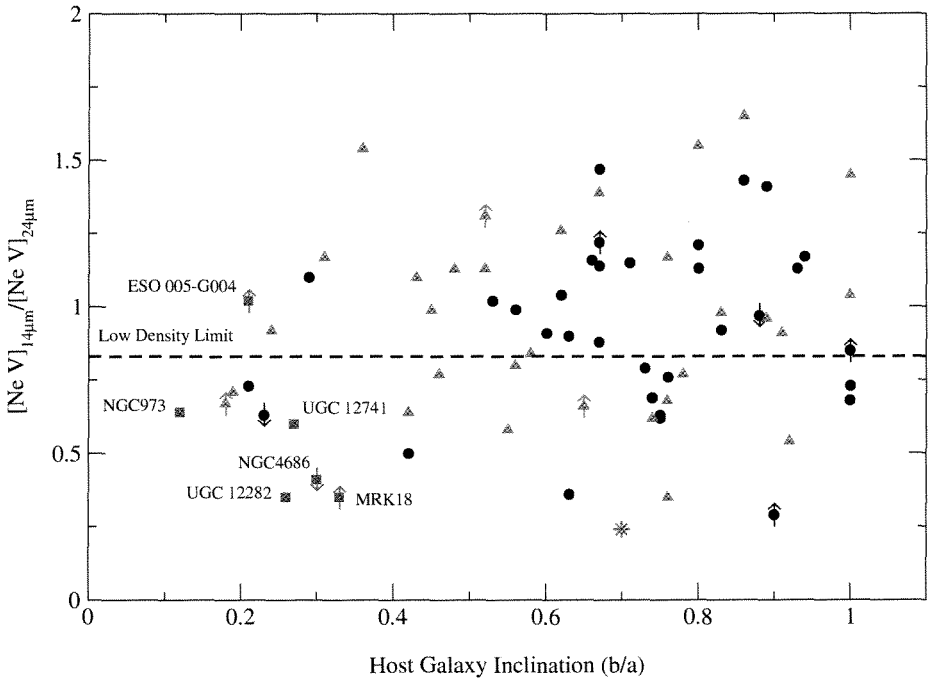

Fig. 8.— The $[NeV]_{24\mu m}$ and $[NeV]_{14\mu m}$ ratios as a function of host galaxy inclination for the BAT sample. The horizontal line shows the low density limit. Note that, while there are AGN with [Ne V] ratios below the low-density limit at all inclinations, there is a larger fraction in that range in highly inclined hosts ($b/a < 0.4$). In particular, all but one of the newly detected BAT AGN reside in inclined hosts, hence host galaxy extinction may be responsible for their lack of AGN signatures in the optical

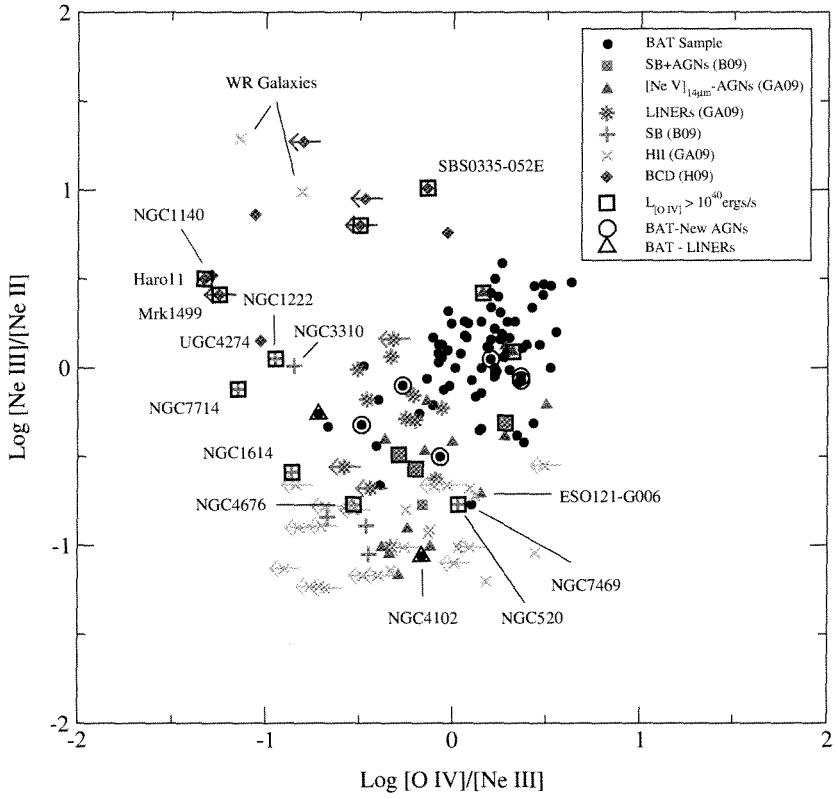

Fig. 9.— [Ne III]/[Ne II] versus [O IV]/[Ne III] for the same sample of sources presented in Figure ??.

Table 1. *Spitzer* IRS High-Resolution Spectroscopy of the BAT sample of AGNs

Name	z[a]	Type[a]	BAT[b]	[Ne II] (12.81μm)	[Ne V] (14.32μm)	[Ne III] (15.56μm)	[Ne V] (24.32μm)	[O IV] (25.89μm)
				Integrated Line Fluxes (10^{-21}W cm^{-2})				
2MASX J05580206-3820043	0.0339	1	3.99 ± 0.37	3.20 ± 0.89	1.89 ± 0.13	4.72 ± 0.14	3.80 ± 0.51	3.69 ± 0.45
3C120	0.0330	1	11.89 ± 0.63	9.19 ± 0.66	17.21 ± 0.28	27.43 ± 0.92	27.63 ± 8.92	116.68 ± 1.22
Ark 120	0.0327	1	7.08 ± 0.57	3.47 ± 0.91	<1.18	4.33 ± 0.79	<1.29	4.03 ± 0.38
Cen A[c]	0.0018	2	92.62 ± 0.71	193.00	23.16	147.65	29.92	131.24
ESO 005-G004	0.0062	···	4.48 ± 0.6	16.64 ± 1.19	0.50 ± 0.12	5.29 ± 0.34	<0.49	4.49 ± 0.19
ESO 033- G002	0.0181	2	2.61 ± 0.45	2.67 ± 0.18	5.57 ± 0.56	8.34 ± 0.56	5.37 ± 0.51	13.85 ± 0.73
ESO 103-G035	0.0133	2	11.14 ± 0.59	30.92 ± 2.07	15.85 ± 3.49	41.62 ± 1.78	10.31 ± 0.87	34.40 ± 0.75
ESO 140-G043	0.0142	1	4.57 ± 0.66	11.41 ± 0.26	7.83 ± 0.70	13.93 ± 0.32	7.95 ± 0.44	27.46 ± 0.35
ESO 323-G077	0.0150	1.2	4.7 ± 0.66	40.16 ± 1.41	5.44 ± 1.61	18.07 ± 1.07	6.19 ± 0.14	25.11 ± 0.62
ESO 362-G018	0.0124	1.5	6.22 ± 0.52	9.94 ± 0.23	3.15 ± 0.37	7.16 ± 0.18	2.75 ± 0.20	10.11 ± 0.37
ESO 417- G006	0.0163	2	3.06 ± 0.46	1.77 ± 0.14	0.42 ± 0.10	2.54 ± 0.07	0.47 ± 0.16	4.04 ± 0.18
F49	0.0202	2	2.93 ± 0.54	39.55 ± 2.93	25.50 ± 2.96	47.12 ± 2.43	12.74 ± 0.36	39.22 ± 2.37
F9	0.0470	1	5.07 ± 0.45	2.91 ± 0.68	<2.66	5.31 ± 0.37	2.74 ± 0.37	6.08 ± 0.26
IC1816	0.0169	1	2.58 ± 0.48	18.36 ± 1.51	6.21 ± 0.61	19.64 ± 1.17	4.34 ± 0.30	16.52 ± 1.81
IC 4329A	0.0161	1.2	33.08 ± 0.62	30.19 ± 2.76	32.79 ± 6.01	65.30 ± 0.95	29.90 ± 1.74	103.58 ± 3.24
IC 486	0.0269	1	3.22 ± 0.7	6.86 ± 0.05	3.30 ± 0.20	6.79 ± 0.21	2.84 ± 0.01	11.19 ± 0.29
IC 5063	0.0113	2	8.59 ± 0.72	28.22 ± 3.34	35.97 ± 1.58	73.67 ± 4.61	25.86 ± 1.20	117.21 ± 11.13
MCG-01-13-025[f]	0.0159	1.2	<4.5	2.87 ± 0.18	<0.18	1.90 ± 0.05	<1.44	0.76 ± 0.18
MCG-05-23-016	0.0085	2	20.77 ± 0.56	18.13 ± 0.42	11.06 ± 0.50	16.96 ± 0.93	11.19 ± 0.26	27.95 ± 7.61
MCG-01-24-012	0.0196	2	4.58 ± 0.51	6.74 ± 0.41	2.90 ± 0.27	6.07 ± 0.36	2.30 ± 0.58	10.07 ± 0.77

Table 1—Continued

Name	z[a]	Type[a]	BAT[b]	[Ne II] (12.81μm)	[Ne V] (14.32μm)	[Ne III] (15.56μm)	[Ne V] (24.32μm)	[O IV] (25.89μm)
				Integrated Line Fluxes (10^{-21}W cm^{-2})				
MCG-02-58-22	0.0469	1.5	10.17 ± 0.57	5.29 ± 0.39	2.80 ± 0.34	9.71 ± 0.16	3.05 ± 0.39	13.74 ± 1.74
MCG-03-34-064	0.0165	1.8	3.15 ± 0.45	57.83 ± 7.29	54.98 ± 5.26	120.13 ± 6.88	35.46 ± 1.92	110.83 ± 9.35
MCG-06-30-015	0.0077	1.2	7.82 ± 0.57	4.20 ± 0.12	6.05 ± 0.76	6.62 ± 0.33	6.62 ± 0.05	23.49 ± 0.81
MRK 3[c]	0.0135	2	15.65 ± 0.61	100.00	64.50	179.00	67.50	214.00
MRK 6[d]	0.0188	1.5	7.61 ± 0.55	28.00 ± 0.23	9.39 ± 0.19	49.34 ± 0.32	10.43 ± 0.21	48.24 ± 0.27
MRK 18[f]	0.0111	···	<3.1	17.04 ± 0.71	0.78 ± 0.01	8.24 ± 0.24	<2.24	2.69 ± 0.14
MRK 79	0.0222	1.2	4.89 ± 0.52	11.29 ± 3.71	9.62 ± 1.07	20.43 ± 0.50	13.16 ± 1.10	39.99 ± 2.68
MRK 335	0.0258	1.2	2.47 ± 0.41	2.10 ± 0.31	1.31 ± 0.11	2.70 ± 0.15	<1.55	6.31 ± 0.17
MRK 348	0.0150	2	13.66 ± 0.56	15.34 ± 0.74	6.90 ± 0.36	20.60 ± 0.79	4.75 ± 0.27	17.87 ± 0.23
MRK 352	0.0149	1	4.16 ± 0.5	0.54 ± 0.08	<0.16	0.34 ± 0.02	<0.23	0.26 ± 0.04
MRK 509	0.0344	1.2	9.44 ± 0.68	11.98 ± 1.06	7.61 ± 1.74	17.32 ± 3.29	7.60 ± 0.10	27.54 ± 0.42
MRK 590[f]	0.0264	1.2	<3.7	5.26 ± 0.46	<3.22	5.42 ± 0.12	<1.23	1.79 ± 0.26
MRK 766	0.0129	1.5	2.42 ± 0.29	24.27 ± 0.94	22.14 ± 0.23	23.52 ± 1.41	18.32 ± 1.60	46.47 ± 0.84
MRK 817	0.0315	1.5	2.21 ± 0.36	4.57 ± 0.88	2.88 ± 0.48	5.51 ± 0.77	4.22 ± 0.73	6.06 ± 0.23
MRK 841	0.0364	1.5	2.93 ± 0.37	3.18 ± 0.18	8.12 ± 0.31	12.46 ± 0.73	6.96 ± 0.33	22.91 ± 1.08
NGC 454[f]	0.0122	2	<2.3	4.70 ± 0.40	3.73 ± 0.14	6.40 ± 0.17	5.54 ± 0.31	15.80 ± 0.85
NGC 513	0.0195	2	2.06 ± 0.43	10.38 ± 1.78	1.52 ± 0.23	4.71 ± 0.32	1.38 ± 0.21	6.69 ± 0.41
NGC 788	0.0136	2	9.33 ± 0.57	6.59 ± 0.11	5.35 ± 0.34	13.60 ± 0.50	8.68 ± 1.28	24.14 ± 0.36
NGC 931	0.0167	1.5	6.56 ± 0.5	5.50 ± 0.59	9.91 ± 2.31	15.94 ± 0.52	13.52 ± 0.58	42.90 ± 0.63
NGC 973	0.0162	···	3.09 ± 0.58	8.03 ± 0.09	2.07 ± 0.18	8.92 ± 0.38	3.21 ± 0.27	14.11 ± 2.64

Table 1—Continued

Name	z[a]	Type[a]	BAT[b]	[Ne II] (12.81μm)	[Ne V] (14.32μm)	[Ne III] (15.56μm)	[Ne V] (24.32μm)	[O IV] (25.89μm)
				Integrated Line Fluxes (10^{-21}W cm^{-2})				
NGC 1052	0.0050	LINER	3.75 ± 0.67	22.22 ± 0.94	0.64 ± 0.03	12.31 ± 0.48	2.69 ± 1.33	2.37 ± 0.10
NGC 1194	0.0136	1.9	3.64 ± 0.6	3.27 ± 0.34	4.48 ± 0.12	8.27 ± 0.41	3.98 ± 0.32	14.39 ± 0.10
NGC 1365	0.0055	1.8	7.19 ± 0.44	161.67 ± 17.48	22.35 ± 1.97	61.06 ± 0.90	38.53 ± 1.50	145.38 ± 8.89
NGC 2110	0.0078	2	35.01 ± 0.7	60.19 ± 5.34	5.22 ± 0.82	47.40 ± 0.71	7.65 ± 0.63	45.71 ± 3.41
NGC 2992	0.0077	2	4.82 ± 0.63	53.65 ± 3.66	32.62 ± 5.38	61.06 ± 1.98	27.81 ± 0.20	114.22 ± 6.44
NGC 3079[c]	0.0037	2	3.44 ± 0.44	104.00	1.04	22.88	<1.56	9.26
NGC 3081	0.0080	2	10.24 ± 0.67	12.62 ± 1.16	12.62 ± 0.81	36.46 ± 1.25	35.79 ± 0.05	119.73 ± 8.42
NGC 3227	0.0039	1.5	14.13 ± 0.5	65.05 ± 6.91	26.23 ± 1.23	74.62 ± 2.00	17.82 ± 0.99	64.91 ± 2.31
NGC 3281	0.0107	2	9.01 ± 0.66	19.94 ± 2.16	47.51 ± 2.75	58.35 ± 2.48	42.15 ± 3.24	174.65 ± 13.25
NGC 3516[d]	0.0088	1.5	12.54 ± 0.45	8.07 ± 0.25	7.88 ± 0.50	17.72 ± 0.33	10.39 ± 0.33	46.92 ± 0.35
NGC 3783	0.0097	1	19.45 ± 0.66	19.82 ± 0.79	19.54 ± 3.44	26.18 ± 0.57	13.82 ± 0.29	39.25 ± 0.07
NGC 4051	0.0023	1.5	4.34 ± 0.35	19.69 ± 0.92	10.17 ± 0.65	16.35 ± 0.44	16.19 ± 2.53	36.95 ± 2.05
NGC 4102	0.0028	LINER	2.58 ± 0.38	349.81 ± 39.88	<8.10	30.44 ± 1.12	<6.29	20.66 ± 7.69
NGC 4138	0.0030	1.9	3.69 ± 0.45	3.23 ± 0.52	0.54 ± 0.10	2.82 ± 0.37	<0.83	2.03 ± 0.18
NGC 4151[c]	0.0033	1.5	62.23 ± 0.46	134.00	77.72	204.35	67.67	236.51
NGC 4235	0.0080	1	2.4 ± 0.55	3.69 ± 0.65	<0.58	3.70 ± 0.54	0.92 ± 0.19	3.77 ± 0.77
NGC 4388	0.0084	2	34.64 ± 0.52	79.74 ± 4.76	45.35 ± 0.84	108.18 ± 1.56	64.10 ± 0.12	311.42 ± 25.79
NGC 4395	0.0011	1.8	3.12 ± 0.41	4.74 ± 0.25	1.47 ± 0.13	7.02 ± 0.58	1.49 ± 0.62	8.16 ± 0.26
NGC 4507	0.0118	2	22.51 ± 0.68	33.73 ± 2.63	12.50 ± 1.39	28.63 ± 2.36	10.72 ± 1.96	36.33 ± 4.14
NGC 4593	0.0090	1	9.79 ± 0.62	8.31 ± 0.30	5.56 ± 1.27	7.89 ± 0.59	8.02 ± 1.96	13.39 ± 2.00

Table 1—Continued

Name	z[a]	Type[a]	BAT[b]	[Ne II] (12.81μm)	[Ne V] (14.32μm)	[Ne III] (15.56μm)	[Ne V] (24.32μm)	[O IV] (25.89μm)
				Integrated Line Fluxes (10^{-21}W cm^{-2})				
NGC 4686	0.0167	···	3.08 ± 0.45	2.13 ± 0.16	<0.22	1.71 ± 0.13	0.53 ± 0.09	0.91 ± 0.30
NGC 526A	0.0191	1.5	5.96 ± 0.51	6.22 ± 1.61	3.94 ± 0.47	9.59 ± 1.10	3.87 ± 0.86	17.34 ± 0.84
NGC 5506	0.0062	1.9	25.64 ± 0.5	91.75 ± 3.31	58.28 ± 3.34	152.13 ± 9.13	63.25 ± 2.40	252.82 ± 2.29
NGC 5548	0.0172	1.5	8.08 ± 0.5	8.93 ± 0.70	1.95 ± 0.10	8.99 ± 0.97	1.73 ± 0.75	12.75 ± 0.80
NGC 5728	0.0094	2	10.54 ± 0.71	30.44 ± 1.81	23.56 ± 0.77	54.76 ± 0.51	28.15 ± 0.56	118.40 ± 7.61
NGC 5995	0.0252	2	4.51 ± 0.61	13.32 ± 1.91	7.60 ± 1.42	9.19 ± 0.59	4.61 ± 0.84	12.20 ± 0.80
NGC 6240[e]	0.0245	2	7.3 ± 0.62	193.10 ± 3.70	5.10 ± 0.90	70.40 ± 2.40	<3.90	27.20 ± 0.70
NGC 6860	0.0149	1	6.5 ± 0.73	5.88 ± 0.11	2.95 ± 0.94	7.50 ± 0.53	2.84 ± 0.21	11.70 ± 0.39
NGC 7172	0.0087	2	18.11 ± 0.7	32.03 ± 2.44	8.99 ± 0.80	15.71 ± 0.69	11.26 ± 0.95	42.60 ± 3.44
NGC 7213	0.0058	1.5	5.75 ± 0.67	27.47 ± 1.33	0.56 ± 0.00	12.77 ± 0.66	<1.94	2.75 ± 0.59
NGC 7314	0.0048	1.9	4.63 ± 0.59	8.97 ± 0.74	16.84 ± 0.60	23.28 ± 0.41	21.92 ± 0.40	69.62 ± 7.82
NGC 7469[c]	0.0163	1.2	6.66 ± 0.44	200.00	11.60	34.00	14.70	43.00
NGC 7582	0.0053	2	7.92 ± 0.55	250.94 ± 3.53	38.02 ± 3.86	104.99 ± 4.37	59.54 ± 6.39	227.65 ± 10.88
NGC 7603	0.0295	1.5	4.7 ± 0.51	9.32 ± 0.72	0.47 ± 0.01	5.07 ± 0.49	<0.38	3.34 ± 0.18
NGC 7682	0.0171	2	2.27 ± 0	5.46 ± 0.25	1.98 ± 0.19	8.07 ± 0.15	3.69 ± 1.46	16.21 ± 0.66
UGC 03601	0.0171	1.5	4.38 ± 0.67	5.26 ± 0.53	2.01 ± 0.12	7.60 ± 0.13	1.79 ± 0.44	13.45 ± 0.65
UGC 06728	0.0065	1.2	2.95 ± 0.37	1.40 ± 0.36	1.16 ± 0.10	1.38 ± 0.05	3.24 ± 0.03	4.61 ± 0.81
UGC 12282	0.0170	···	2.49 ± 0.5	2.08 ± 0.28	0.50 ± 0.01	1.76 ± 0.05	1.44 ± 0.20	4.07 ± 0.37
UGC 12741	0.0174	···	4.00 ± 0.59	1.72 ± 0.07	0.39 ± 0.06	1.55 ± 0.05	0.65 ± 0.06	3.58 ± 0.38

[a]AGN type and redshift values are taken from NED.

[b]The BAT flux is presented in units of 10^{-11}ergs $s^{-1}cm^{-2}$.

[c]Weedman et al. (2005)

[d]Tommasin et al. (2008)

[e]Armus et al. (2006)

[f]From the 9-month BAT survey (Tueller et al. 2008)

Table 2. Statistical Analysis for the Different Relationships Between the Mid-infrared Emission Lines and BAT Luminosity for the Sample

Variables	ρ_s	P_ρ	τ	P_τ	τ_p	σ	$P_\tau(p)$
All Sample							
BAT-[Ne II]	0.66	$< 1 \times 10^{-6}$	0.49	$< 1 \times 10^{-6}$	0.37	0.07	$< 1 \times 10^{-6}$
BAT-[Ne III]	0.76	$< 1 \times 10^{-6}$	0.58	$< 1 \times 10^{-6}$	0.45	0.06	$< 1 \times 10^{-6}$
BAT-[O IV]	0.65	$< 1 \times 10^{-6}$	0.48	$< 1 \times 10^{-6}$	0.36	0.06	$< 1 \times 10^{-6}$
BAT-[Ne v]	0.63	$< 1 \times 10^{-6}$	0.50	$< 1 \times 10^{-6}$	0.38	0.07	$< 1 \times 10^{-6}$
[NeIII]-[NeII]	0.89	$< 1 \times 10^{-6}$	0.74	$< 1 \times 10^{-6}$	0.68	0.06	$< 1 \times 10^{-6}$
[O IV]-[Ne II]	0.80	$< 1 \times 10^{-6}$	0.60	$< 1 \times 10^{-6}$	0.54	0.06	$< 1 \times 10^{-6}$
[O IV]-[Ne III]	0.94	$< 1 \times 10^{-6}$	0.80	$< 1 \times 10^{-6}$	0.76	0.06	$< 1 \times 10^{-6}$
$[Ne\ V]_{14}$[Ne II]	0.77	$< 1 \times 10^{-6}$	0.59	$< 1 \times 10^{-6}$	0.53	0.06	$< 1 \times 10^{-6}$
$[Ne\ V]_{14}$[Ne III]	0.91	$< 1 \times 10^{-6}$	0.79	$< 1 \times 10^{-6}$	0.75	0.06	$< 1 \times 10^{-6}$
$[Ne\ V]_{14}$[O IV]	0.94	$< 1 \times 10^{-6}$	0.80	$< 1 \times 10^{-6}$	0.77	0.06	$< 1 \times 10^{-6}$
$[Ne\ V]_{24}$-$[Ne\ V]_{14}$	0.93	$< 1 \times 10^{-6}$	0.80	$< 1 \times 10^{-6}$	0.77	0.06	$< 1 \times 10^{-6}$
Seyfert 1 Galaxies							
BAT-[Ne II]	0.75	$< 1 \times 10^{-6}$	0.60	$< 1 \times 10^{-6}$	0.37	0.11	$< 9.12 \times 10^{-4}$
BAT-[Ne III]	0.82	$< 1 \times 10^{-6}$	0.66	$< 1 \times 10^{-6}$	0.41	0.12	$< 1.08 \times 10^{-3}$
BAT-[O IV]	0.72	$< 1 \times 10^{-6}$	0.56	$< 1 \times 10^{-6}$	0.33	0.11	$< 3.43 \times 10^{-3}$
BAT-[Ne V]	0.61	$< 2.32 \times 10^{-4}$	0.52	$< 1 \times 10^{-6}$	0.32	0.12	$< 7.52 \times 10^{-3}$
[O IV]-[Ne II]	0.84	$< 1 \times 10^{-6}$	0.66	$< 1 \times 10^{-6}$	0.54	0.09	$< 1 \times 10^{-6}$
[O IV]-[Ne III]	0.93	$< 1 \times 10^{-6}$	0.79	$< 1 \times 10^{-6}$	0.71	0.08	$< 1 \times 10^{-6}$
$[Ne\ V]_{14}$[Ne II]	0.77	$< 1 \times 10^{-6}$	0.61	$< 1 \times 10^{-6}$	0.49	0.08	$< 1 \times 10^{-6}$
$[Ne\ V]_{14}$[Ne III]	0.86	$< 1 \times 10^{-6}$	0.75	$< 1 \times 10^{-6}$	0.67	0.08	$< 1 \times 10^{-6}$
$[Ne\ V]_{14}$[O IV]	0.92	$< 1 \times 10^{-6}$	0.78	$< 1 \times 10^{-6}$	0.72	0.08	$< 1 \times 10^{-6}$

Table 2—Continued

Variables	ρ_s	P_ρ	τ	P_τ	τ_p	σ	$P_\tau(p)$
[Ne V]$_{24}$-[Ne V]$_{14}$	0.92	$< 1 \times 10^{-6}$	0.81	$< 1 \times 10^{-6}$	0.77	0.08	$< 1 \times 10^{-6}$
Seyfert 2 Galaxies							
BAT-[Ne II]	0.63	$< 7.13 \times 10^{-5}$	0.48	$< 6.79 \times 10^{-5}$	0.40	0.11	$< 5.47 \times 10^{-4}$
BAT-[Ne III]	0.71	$< 1 \times 10^{-6}$	0.55	$< 1 \times 10^{-6}$	0.45	0.10	$< 1.91 \times 10^{-5}$
BAT-[O IV]	0.56	$< 6.04 \times 10^{-4}$	0.42	$< 4.94 \times 10^{-4}$	0.33	0.10	$< 1.97 \times 10^{-3}$
BAT-[Ne V]	0.65	$< 2.00 \times 10^{-4}$	0.49	$< 1 \times 10^{-6}$	0.38	0.11	$< 8.43 \times 10^{-4}$
[O IV]-[Ne II]	0.76	$< 1 \times 10^{-6}$	0.59	$< 1 \times 10^{-6}$	0.54	0.09	$< 1 \times 10^{-6}$
[O IV]-[Ne III]	0.94	$< 1 \times 10^{-6}$	0.81	$< 1 \times 10^{-6}$	0.79	0.08	$< 1 \times 10^{-6}$
[Ne V]$_{14}$[Ne II]	0.73	$< 3.60 \times 10^{-5}$	0.58	$< 1 \times 10^{-6}$	0.52	0.09	$< 1 \times 10^{-6}$
[Ne V]$_{14}$[Ne III]	0.94	$< 1 \times 10^{-6}$	0.83	$< 1 \times 10^{-6}$	0.80	0.10	$< 1 \times 10^{-6}$
[Ne V]$_{14}$[O IV]	0.94	$< 1 \times 10^{-6}$	0.80	$< 1 \times 10^{-6}$	0.78	0.09	$< 1 \times 10^{-6}$
[Ne V]$_{24}$-[Ne V]$_{14}$	0.92	$< 1 \times 10^{-6}$	0.80	$< 1 \times 10^{-6}$	0.78	0.09	$< 1 \times 10^{-6}$

Note. — ρ_s is the Spearman rank order correlation coefficient with its associated null probability, P_ρ. τ represents the generalized Kendall's correlation coefficient for censored data and τ_p is the Kendall's coefficient for partial correlation with censored data. P_τ and $P_{\tau,p}$ are the null probabilities for the generalized and partial Kendall's correlation test, respectively, together with the calculated variance, σ, for Kendall τ_p. We have used a partial correlation test to exclude the effect of redshift (distance) in the Luminosity-Luminosity correlations.

Table 3. Statistical Analysis Between Seyfert 1 and Seyfert 2 Galaxies

	Seyfert 1			Seyfert 2			
	Measurements Available	Median	Standard Deviation	Measurements Available	Median	Standard Deviation	P_{K-S} (%)
LogBAT/[O IV]	38	2.53	0.08	33	2.40	0.08	2.4
LogBAT/[Ne III]	38	2.77	0.06	33	2.50	0.07	9.0
LogBAT/[Ne V]$_{14.34}$	32	3.00	0.07	33	2.91	0.09	26.1
LogBAT/[Ne II]	38	2.94	0.07	33	2.66	0.08	2.8
[Ne III]/[Ne II]	38	1.2	0.1	33	1.4	0.1	54.8
[O IV]/[Ne II]	38	1.8	0.4	33	1.7	0.4	84.5
[O IV]/[Ne III]	38	1.5	0.1	33	1.7	0.1	91.4
L_{BAT}	38	43.6	0.1	33	43.3	0.1	18.1
$L_{[O\ IV]}$	38	41.0	0.1	33	41.0	0.1	86.4
$L_{[NeV]_{24.32}}$	31	40.5	0.1	30	40.5	0.1	40.2
$L_{[Ne\ III]}$	38	40.9	0.1	33	40.8	0.1	98.4
$L_{[Ne\ V]_{14.32}}$	32	40.5	0.1	33	40.4	0.2	98.7
$L_{[Ne\ II]}$	38	40.7	0.1	33	40.8	0.1	96.6

Note. — The last column, P_{K-S}, represents the Kolmogorov-Smirnov (K-S) test null probability. Upper limits for the [Ne V] fluxes are not included. This table also includes information about the numbers of Seyfert 1 and Seyfert 2 galaxies, median values and standard deviations of the mean for the measured quantities.

Table 4. Linear regressions for the Mid-infrared and 14-195 keV luminosities

Log X - Log Y	Y=aX+b	
	a	b
All Sample		
BAT- [Ne II]	0.72 ± 0.11	9.60 ± 4.85
BAT-[Ne III]	0.88 ± 0.06	2.58 ± 2.70
BAT-[O IV]	0.93 ± 0.08	0.42 ± 3.32
BAT-[Ne V]$_{14}$	1.00 ± 0.10	-3.28 ± 4.51
[O IV]-[Ne II]	0.85 ± 0.07	5.83 ± 2.67
[O IV]-[Ne III]	0.90 ± 0.04	3.96 ± 1.65
[Ne III]-[Ne II]	0.94 ± 0.04	2.22 ± 1.80
[Ne V]$_{14}$[Ne II]	0.67 ± 0.06	13.46 ± 2.35
[Ne V]$_{14}$[Ne III]	0.82 ± 0.04	7.80 ± 1.43
[Ne V]$_{14}$[O IV]	0.93 ± 0.03	3.59 ± 1.20
[Ne V]$_{24}$-[Ne V]$_{14}$	0.89 ± 0.05	4.52 ± 2.20
Seyfert 1 Galaxies		
BAT- [Ne II]	0.77 ± 0.08	7.08 ± 3.69
BAT-[Ne III]	0.93 ± 0.08	0.43 ± 3.68
BAT-[O IV]	0.93 ± 0.11	0.37 ± 5.00
BAT-[Ne V]$_{14}$	0.91 ± 0.15	0.79 ± 6.65
[O IV]-[Ne II]	0.84 ± 0.10	6.21 ± 3.91
[O IV]-[Ne III]	0.91 ± 0.07	3.57 ± 2.78
[Ne III]-[Ne II]	0.92 ± 0.06	3.03 ± 2.56
[Ne V]$_{14}$[Ne II]	0.74 ± 0.09	10.65 ± 3.76

Table 4—Continued

Log X - Log Y	Y=aX+b	
	a	b
[Ne V]$_{14}$[Ne III]	0.90 ± 0.06	4.44 ± 2.53
[Ne V]$_{14}$[O IV]	1.00 ± 0.05	0.62 ± 2.16
[Ne V]$_{24}$-[Ne V]$_{14}$	1.02 ± 0.05	-0.69 ± 1.50
Seyfert 2 Galaxies		
BAT- [Ne II]	0.94 ± 0.15	0.15 ± 6.56
BAT-[Ne III]	0.99 ± 0.10	-1.82 ± 4.42
BAT-[O IV]	1.00 ± 0.13	-2.17 ± 5.72
BAT-[Ne V]$_{14}$	1.10 ± 0.12	-7.10 ± 5.28
[O IV]-[Ne II]	0.98 ± 0.10	0.48 ± 3.89
[O IV]-[Ne III]	0.96 ± 0.05	1.47 ± 2.14
[Ne III]-[Ne II]	1.02 ± 0.05	-1.01 ± 2.18
[Ne V]$_{14}$[Ne II]	0.89 ± 0.09	4.78 ± 3.62
[Ne V]$_{14}$[Ne III]	0.87 ± 0.05	5.73 ± 2.11
[Ne V]$_{14}$[O IV]	0.90 ± 0.04	4.45 ± 1.50
[NevV]$_{24}$-[Ne V]$_{14}$	1.07 ± 0.04	-2.97 ± 1.48

Note. — $\log X$ and $\log Y$ represent the independent and dependent variables, respectively. a and b represent the regression coefficient (slope) and re-

gression constant (intercept) respectively. For the relationship between the 14-195 keV and mid-infrared luminosities we used the ordinary least-square regression of the dependent variable, Y, against the independent variable X, OLS($Y|X$). For the relationship between the mid-infrared emission line luminosities we used the OLS bisector method which treat the variables symmetrically (see Isobe et al. 1990, for a review). When censored data was present we used the EM and the Buckley-James (BJ) method, if censored data was present in both variables (e.g., the $[\mathrm{Ne\ V}]_{14} - [\mathrm{NeV}]_{24}$ relationship) the Schmitt's binned method was used (Isobe et al. 1986; Isobe & Feigelson 1990). The results from the EM and BJ methods agree within their estimated errors, therefore, for the sake of simplicity, we present only the values from the EM regression.